High-dimensional analysis reveals a distinct population of adaptive-like tissue-resident NK cells in human lung

Nicole Marquardt[1*], Marlena Scharenberg[1], Jeffrey E. Mold[2], Joanna Hård[2], Eliisa Kekäläinen[3,4], Marcus Buggert[1], Son Nguyen[5,6], Jennifer N. Wilson[1], Mamdoh Al-Ameri[7], Hans-Gustaf Ljunggren[1], Jakob Michaëlsson[1]

Running title: Adaptive-like human lung tissue-resident NK cells

Affiliations:

[1]Center for Infectious Medicine, Department of Medicine, Karolinska Institutet, Stockholm, Sweden

[2]Department of Cell and Molecular Biology, Karolinska Institutet, Stockholm, Sweden

[3]Translational Immunology Research Program & Department of Bacteriology and Immunology, University of Helsinki, Finland

[4]HUSLAB, Division of Clinical Microbiology, Helsinki University Hospital, Helsinki, Finland,

[5]Department of Microbiology, Perelman School of Medicine, University of Pennsylvania, Philadelphia, PA, USA

[6]Institute for Immunology, Perelman School of Medicine, University of Pennsylvania, Philadelphia, PA, USA

[7]Thoracic Surgery, Department of Molecular Medicine and Surgery, Karolinska Institutet, Karolinska University Hospital, Stockholm, Sweden

25 ***Corresponding author:** Nicole Marquardt, Center for Infectious Medicine,
26 Department of Medicine, Karolinska Institutet, Karolinska University Hospital, 141 86
27 Stockholm, Sweden; E-mail: nicole.marquardt@ki.se, Phone: +46-8-58589791 Fax:
28 +468-7467637

Abstract

The concept of adaptive-like "memory" NK cells has been extensively investigated in recent years. In humans, NK cells with adaptive-like features have been identified in peripheral blood and liver of cytomegalovirus (CMV)-seropositive individuals. The human lung is a major target organ for infections and is also a significant reservoir for CMV. However, it remains unknown whether adaptive-like NK cells can be found in this organ. Using RNAseq and flow cytometry analysis, we here identify a novel adaptive-like $KIR^{+}NKG2C^{+}$ NK cell subset with a $CD49a^{+}CD56^{bright}CD16^{-}$ tissue-resident (tr)NK cell phenotype in human lung and in peripheral blood. Adaptive-like lung trNK cells were found to be present independently of adaptive-like $CD56^{dim}CD16^{+}$ NK cells, to be hyperresponsive towards target cells, and to exhibit signs of metabolic reprogramming. In conclusion, adaptive-like trNK cells constitute a novel subset of human lung NK cells, likely contributing to unique defense mechanisms in context of infection at this site.

Key words: NK cells, adaptive, lung, tissue-resident

Abbreviations:

Eomes: Eomesodermin

FITC: Fluorescein isothiocyanate

HCMV: Human cytomegalovirus

ILC: Innate lymphoid cell

KIR: Killer cell immunoglobulin-like receptor

NK: Natural killer

PE: Phycoerythrin

ROS: Reactive oxygen species

54 **Introduction**

55 Natural killer (NK) cells are a crucial part of the innate immune system. They
56 eliminate virus-infected and malignant cells, and produce proinflammatory cytokines
57 including IFN-γ and TNF. In recent years, the concept of adaptive-like or "memory"
58 NK cells has emerged from studies in mice[1-4] and humans[5-10]. These cells share a
59 distinct phenotype and increased target cell responsiveness as well as having features
60 of longevity [11].

61 Most studies of human adaptive-like NK cells have focused on subsets of
62 NKG2C^{+}(KIR^{+})CD56^{dim}CD16^{+} NK cells, originally found to be expanded and stably
63 imprinted in peripheral blood of approximately 30-40% of human CMV (HCMV)-
64 seropositive individuals[5,10]. Adaptive-like CD56^{dim}CD16^{+} NK cells in human
65 peripheral blood have a distinctive phenotypic[5,10], epigenetic[8,9], and functional[8-10]
66 profile compared to conventional NK cells and have been suggested to contribute to
67 immunity against HCMV[1,12]. We recently described a subset of tissue-resident
68 CD49a^{+}KIR^{+}NKG2C^{+}CD56^{bright}CD16^{-} NK cells in the human liver[7], potentially
69 representing a counterpart to the CD49a^{+}DX5^{-} adaptive-like tissue-resident NK (trNK)
70 cells in murine liver. In virus-independent settings, murine hepatic CD49a^{+}DX5^{-}
71 adaptive-like NK cells have been shown to mediate contact hypersensitivity[3]. Virus-
72 driven antigen-specific NK cell memory has been identified in mouse models following
73 infection with MCMV[1,13,14], influenza A virus (IAV)[4,15,16], vesicular stomatitis virus
74 (VSV)[4], vaccinia virus[17], HIV-1[4], and herpes simplex virus 2 (HSV-2)[16], and after
75 immunization with simian immunodeficiency virus (SIV) in rhesus macaques[18].
76 Together, current data indicate that viral infections might drive and shift the
77 development of unique NK cell subsets in different compartments.

78 The human lung is a frequent site of acute infections, including infections with
79 viruses such as influenza virus, respiratory syncytial virus (RSV), and HCMV, as well
80 as serving as a reservoir for latent HCMV infection[19]. Although human CD56^{dim}CD16^{+}
81 lung NK cells are hyporesponsive to *ex vivo* target cell stimulation[20], exposure of NK
82 cells to virus-infected cells is likely to result in functional NK cell priming. Indeed,
83 increased polyfunctional responses have been observed in CD16^{-} lung NK cells
84 following *in vitro* infection with IAV[21,22].

85 Here, we identify a novel adaptive-like CD49a^{+}KIR^{+}NKG2C^{+}CD56^{bright}CD16^{-}
86 NK cell population in the human lung with a tissue-resident phenotype. In donors with
87 expansions of adaptive-like lung trNK cells, small but detectable frequencies of similar
88 NK cells were detected in paired peripheral blood. While adaptive-like
89 KIR^{+}NKG2C^{+}CD56^{dim}CD16^{+} NK cells (as commonly identified in peripheral blood of
90 HCMV-seropositive donors) and CD49a^{+}KIR^{+}NKG2C^{+}CD56^{bright}CD16^{-} adaptive-like
91 lung and blood NK cells shared a common core gene signature, we identified several
92 unique features of each population indicating that they may represent separate
93 developmental lineages. Notably, NK cells from donors with an adaptive-like trNK cell
94 expansion in the lung were hyperresponsive towards target cells and expressed gene
95 sets enriched for metabolic reprogramming. Together,
96 CD49a^{+}KIR^{+}NKG2C^{+}CD56^{bright}CD16^{-} trNK cells in the human lung represent a novel
97 lineage of adaptive-like NK cells with potentially significant implications in lung
98 surveillance and lung-associated pathologies.

99 **Results**

100 *Adaptive-like NK cells can be identified in human lung*

101 We first set out to investigate whether expansions of KIR^{+}NKG2C^{+} adaptive-
102 like NK cells could be identified in the human lung. The majority of NK cells in the
103 lung are phenotypically similar to NK cells found in peripheral blood (CD69^{-}
104 CD56^{dim}CD16^{+}), suggesting that these cells may recirculate between this organ and
105 peripheral blood[20]. Accordingly, KIR^{+}NKG2C^{+}CD56^{dim}CD16^{+} NK cells could be
106 identified not only in peripheral blood but also in the lung (Fig. 1a). Surprisingly, KIR
107 and NKG2C were also co-expressed on CD56^{bright}CD16^{-} lung NK cells, with varying
108 frequencies between donors (Fig. 1b, c) (see Supplementary Fig. 1a for the gating
109 strategy to identify KIR^{+}NKG2C^{+}CD56^{bright}CD16^{-} and CD56^{dim}CD16^{+} NK cells). In
110 several donors the frequencies of KIR^{+}NKG2C^{+}CD56^{bright}CD16^{-} NK cells in human
111 lung vastly exceeded those previously described in the liver[7], with up to 98% of
112 CD56^{bright}CD16^{-} lung NK cells co-expressing KIR and NKG2C (Fig. 1 a, b).

113 Next, we assessed phenotypic features of KIR^{+}NKG2C^{+}CD56^{bright}CD16^{-} lung
114 NK cells in an unbiased manner. Uniform manifold approximation and expression
115 (UMAP) analysis revealed a distinct subset of cells with an expression pattern
116 consistent with adaptive-like NK cells found in peripheral blood and liver, including
117 low expression of Siglec-7 and CD161, and high expression of NKG2C, KIRs, and
118 CD2[7,8,23,24] (Fig. 1d). Unlike KIR^{+}NKG2C^{+}CD56^{dim}CD16^{+} NK cells,
119 KIR^{+}NKG2C^{+}CD56^{bright}CD16^{-} NK cells expressed lower levels of CD45RA and
120 NKp80, and higher levels of CD8 (Fig. 1d). In addition to these expression patterns,
121 manual analysis of individual samples additionally confirmed low expression of ILT2
122 and FcεR1γ, as compared to KIR^{+}NKG2C^{+}CD56^{dim}CD16^{+} lung NK cells (Fig. 1e, f).
123 Furthermore, KIR^{+}NKG2C^{+}CD56^{bright}CD16^{-} lung NK cells displayed higher

124 expression of Eomes and NKG2A, but no significant differences in T-bet expression.
125 Together, our data reveal the presence of a unique adaptive-like NK cell subset, herein
126 identified as KIR^{+}NKG2C^{+}CD56^{bright}CD16^{-}, in the human lung, which is distinct from
127 adaptive-like CD56^{dim}CD16^{+} NK cells previously described in peripheral blood.
128
129 *Adaptive-like NK cell expansions in human lung are tissue-resident*
130 Tissue-resident NK cells in human lung are characterized by expression of
131 CD69 and the integrins CD49a and CD103[21,25]. Strikingly, the vast majority of the
132 distinct population of NKG2C^{+}CD56^{bright}CD16^{-} NK cells identified by UMAP analysis
133 co-expressed CD69 (80%) and CD49a (77%), and a substantial proportion (38%) also
134 co-expressed CD103 (Fig. 2a, b), suggesting that this population represented an
135 adaptive-like trNK cell subset. KIR^{+}NKG2C^{+} NK cells co-expressing any of these
136 markers were mainly CD56^{bright}CD16^{-} (Fig. 2c, d), further demonstrating that they are
137 clearly distinct from adaptive-like CD56^{dim}CD16^{+} NK cells.
138 To further characterize adaptive-like trNK cells in the lung we compared the
139 gene expression profiles of sorted adaptive KIR^{+}NKG2C^{+} and non-adaptive KIR^{-}
140 NKG2C^{-} trNK cells in human lung using RNA sequencing (Fig. 2e, f; see sorting
141 strategy in Supplementary figure 1b, c). 102 genes were differentially expressed
142 ($p<0.05$, log2FC>1), including several *KIR* genes, *CD8A*, *GPR183, IRF8* and *SH2D1B*
143 (EAT2), and genes encoding for the transcription factors MafF (*MAFF*) and ZNF498
144 (*ZSCAN25*). GPR183 has been demonstrated to be crucial for tissue-specific migration
145 of innate lymphoid cells[26], while EAT2 expression has previously been shown to be
146 downregulated in adaptive-like CD56^{dim}CD16^{+} NK cells[8]. Interestingly, while
147 upregulation of both *IRF8* and *THEMIS2* has been reported to be essential for NK cell-
148 mediated responses against MCMV infection[27,28], gene expression of both molecules

149 was low in adaptive-like trNK cells in human lung (Fig. 2e). Furthermore,
150 approximately one third of the differentially expressed genes in adaptive-like lung trNK
151 cells were also differentially expressed in adaptive-like CD57^{+}NKG2C^{+}CD56^{dim}CD16^{+}
152 NK cells in peripheral blood (GSE117614)[29], including *KLRC2* (NKG2C), *KLRC3*
153 (NKG2E), *IL5RA*, *GZMH*, *ITGAD* (CD11d), *RGS9*, *RGS10*, and *KLRB1* (CD161),
154 *KLRC1* (NKG2A), *KLRF1* (NKp80), *TMIGD2*, *IL18RAP*, *FCER1G*, *MLC1*, *CLIC3*
155 and *TLE1* (Fig. 2f).

156 Adaptive-like NK cells in peripheral blood and in the human liver commonly
157 have a distinct KIR expression profile which is dominated by KIRs that bind to self-
158 HLA class I (self-KIRs)[7,10,30]. In the lung, analysis of single KIR expression on CD16^{-}
159 and CD16^{+} NK cell subsets in donors with high frequencies of adaptive-like lung trNK
160 cells revealed that the latter subset displays unique KIR expression patterns compared
161 to CD16^{+} NK cells in blood or lung (Fig. 2g-i; Supplementary Fig. 1d for the gating
162 strategy). High expression of KIRs on the adaptive-like trNK cells was limited to self-
163 KIR, identical to the phenotype described for adaptive-like NK cells in liver and
164 peripheral blood. Notably, even in a donor with adaptive-like NK cell expansions of
165 both trNK cells and CD56^{dim}CD16^{+} NK cells (Fig. 2g), the KIR-expression profile
166 differed between the two subsets.

167 Together, CD49a^{+}KIR^{+}NKG2C^{+}CD56^{bright}CD16^{-} trNK cells in the human lung
168 exhibit a unique profile of activating and inhibitory NK cell receptors (e.g. NKG2A,
169 KIR, NKp80), as well as adaptor, signaling, and effector molecules (FcεR1γ, SH2D1B,
170 granzyme H). This indicates that these are bona fide adaptive-like trNK cells distinct
171 from adaptive-like CD56^{dim}CD16^{+} NK cells, demonstrating the presence of a yet
172 unexplored NK cell population in the human lung.

173

174 *Lung adaptive-like trNK cells are hyperresponsive to target cells*

175 In order to determine whether adaptive-like lung trNK cells differ from non-
176 adaptive CD49a$^-$KIR$^-$NKG2C$^-$CD56^{bright}CD16$^-$ lung trNK cells, we compared
177 expression levels of genes associated with functional competence (Fig. 3a). Gene
178 expression in adaptive-like trNK cells was higher for *IFNG*, *IL33*, *XCL1* and *GZMH*
179 (granzyme H), and lower for *GNLY* (granulysin), *GZMA* (granzyme A), *GZMK*
180 (granzyme K), *IL2RB* (CD122) and *IL18RAP* as compared to non-adaptive lung trNK
181 cells (Fig. 3a).

182 On the protein level, expression levels of perforin were similar in non-adaptive and
183 adaptive-like trNK cells (Fig. 3b, c), consistent with previous results comparing CD49a$^-$
184 and CD49a$^+$ lung NK cells[25]. In contrast, adaptive-like trNK cells expressed elevated
185 levels of granzyme B as compared to non-adaptive trNK cells (Fig. 3b, c). Expression
186 of granzyme B in adaptive-like trNK cells indicated a potential cytotoxic function in
187 this particular subset, despite lung NK cells generally being characterized as
188 hyporesponsive to target cell stimulation[20,21]. Intriguingly, NK cells from donors with
189 an expansion of adaptive-like trNK cells in the lung degranulated stronger and produced
190 more TNF compared to those from donors without such expansions (Fig. 3d). In
191 particular NK cells co-expressing CD49a and KIR degranulated strongly and produced
192 high levels of TNF upon target cell stimulation (Fig. 3d-f). This hyperresponsiveness
193 of adaptive-like lung trNK cells was independent from co-expression of CD103, since
194 similar activation levels were observed between CD49a$^+$CD103$^-$ and CD49a$^+$CD103$^+$
195 KIR$^+$NKG2C$^+$ NK cells (Fig. 3f-h). Blood NK cells from donors with expanded
196 adaptive-like lung trNK cells also responded stronger to target cells as compared to
197 donors without such expansions (Fig. 3f-h). Taken together, these results revealed that
198 the presence of expanded adaptive-like trNK cells in the lung is linked to

199 hyperresponsivity towards target cells, implicating a role of these cells in active
200 immune regulation within the lung.
201
202 *Adaptive-like CD49a^{+}KIR^{+}NKG2C^{+}CD56^{bright}CD16^{-} NK cells can be identified in*
203 *matched peripheral blood*
204 As a hallmark of tissue-resident cells, CD49a is commonly expressed on subsets
205 of T cells and NK cells in diverse non-lymphoid compartments such as the lung[21,22,25,31],
206 liver[7], skin[32], uterus[33], intestine[34], but not in peripheral blood. Intriguingly, however,
207 we identified a small subset of CD49a^{+}KIR^{+}NKG2C^{+} NK cells within the CD16^{-} NK
208 cell population in peripheral blood of donors harboring expansions of adaptive-like
209 trNK cells in the lung (Fig. 4a, b). The frequencies of CD49a^{+}KIR^{+}NKG2C^{+}CD16^{-} NK
210 cells in peripheral blood were considerably lower as compared to adaptive-like lung
211 trNK cells and adaptive-like CD56^{dim}CD16^{+} lung and blood NK cells, respectively (Fig.
212 4b). However, we identified expansions as outliers also in CD49a^{+}KIR^{+}NKG2C^{+}CD16^{-}
213 blood NK cells (Fig. 4b; see gating strategy in Supplementary Fig. 1e). In detail, we
214 found that 18.6% and 25.6% of all donors had an expansion of adaptive-like trNK cells
215 in lung and CD49a^{+}KIR^{+}NKG2C^{+}CD16^{-} NK cells in peripheral blood, respectively. In
216 comparison, 20.9% and 15.1% of all donors had an expansion of adaptive-like
217 CD56^{dim}CD16^{+} NK cells in lung and blood, respectively (Fig. 4b). Interestingly,
218 expansions of adaptive-like CD56^{bright}CD16^{-} and CD56^{dim}CD16^{+} NK cells were
219 virtually mutually exclusive in donors (Fig. 4c). However, there was a substantial
220 overlap within each of these subsets between lung and peripheral blood (Fig. 4c),
221 suggesting that expansions of these distinct adaptive-like NK cell subsets are
222 independent from each other. We next analyzed the phenotype of
223 CD49a^{+}KIR^{+}NKG2C^{+}CD56^{bright}CD16^{-} blood NK cells and found intermediate

224 expression of CD57 with relatively low co-expression of NKG2A (Fig. 4d, e).
225 Furthermore, CD49a^{+}KIR^{+}NKG2C^{+}CD56^{bright}CD16^{-} blood NK cells differed from
226 their counterpart in lung by low expression of both CD69 and CD103 (Fig. 4e, d).
227 Taken together, these results demonstrate the presence of a novel
228 CD49a^{+}KIR^{+}NKG2C^{+}CD16^{-} NK cell subset in the peripheral blood of a subset of
229 donors emerging independently from adaptive-like CD56^{dim}CD16^{+} NK cells.
230
231 *Peripheral blood CD49a^{+}KIR^{+}NKG2C^{+}CD56^{bright}CD16^{-} NK cells share features with*
232 *lung trNK cells and adaptive-like NK cells*
233 The presence of adaptive-like lung trNK cells in patients undergoing surgery
234 for suspected lung cancer did not significantly correlate with any demographical or
235 clinical parameters including age, gender, cigarette smoking, COPD, the type of lung
236 tumor, survival, lung function, or HCMV IgG concentrations in plasma (Supplementary
237 Fig. 2a-f). Therefore, we next assessed whether CD49a^{+}KIR^{+}NKG2C^{+}CD56^{bright}CD16^{-}
238 NK cells could also be identified in the blood of unrelated healthy blood donors. Indeed,
239 we found KIR^{+}NKG2C^{+} NK cells co-expressing CD49a in the CD56^{bright}CD16^{-} NK
240 cell subset in 16% of the blood donors (Fig. 5a, b). Within the CD56^{bright}CD16^{-} NK cell
241 subset, KIR^{+}NKG2C^{+} NK cells were almost exclusively detected in the CD49a^{+}
242 population (Fig. 5c), suggesting that this subset is a population distinct from activated
243 NK cells that have lost expression of CD16. Hence, we next sought to determine the
244 phenotypic profile of healthy blood CD49a^{+}KIR^{+}NKG2C^{+}CD56^{bright}CD16^{-} NK cells.
245 UMAP analysis of CD56^{bright}CD16^{-} NK cells from donors with CD49a^{+} NK cells in the
246 blood revealed a strong separation of the CD49a^{+} NK cell subset co-expressing KIR
247 and NKG2C based on lower expression or lack of CD69, CD45RA, CD57, CD38,
248 NKp80, and TIM-3 as well as high expression of CD8, CXCR3 and granzyme B on

249 CD49a^{+}KIR^{+}NKG2C^{+} NK cells (Fig. 5d). This phenotype could be confirmed in
250 individual samples (Fig. 5e). Interestingly, strong expression of CXCR6 could be
251 identified on CD69^{+}, but not on CD49a^{+}KIR^{+}NKG2C^{+}CD56^{bright}CD16^{-} NK cells,
252 indicating that this NK cell subset depends on other chemokine receptors such as
253 CXCR3 for tissue homing.

254 To gain further insight into the blood CD49a^{+}KIR^{+}CD56^{bright}CD16^{-} NK cells,
255 we sorted this subset and compared it to sorted blood CD49a^{-}KIR^{-}CD56^{bright}CD16^{-} NK
256 cells using RNAseq (Fig. 6a, see Supplementary Fig. 1c for gating strategy). We next
257 investigated whether gene expression differences in CD49a^{+}KIR^{+}CD56^{bright}CD16^{-} NK
258 cells indicated a different functional profile. Blood CD49a^{+}KIR^{+}CD56^{bright}CD16^{-} NK
259 cells expressed particularly higher levels of *CCL5*, *LAMP1, GZMH* and *GNLY*, and
260 lower levels of *XCL1*, *HIF1A*, *IL2RB*, and I*L18RAP* (Fig. 5f). Therefore, blood
261 CD49a^{+}KIR^{+}NKG2C^{+}CD56^{bright}CD16^{-} NK cells and adaptive-like lung trNK cells
262 (Fig. 3a) shared a common gene expression pattern for *CCL5*, *GZMH*, *IL2RB* and
263 *IL18RAP*, indicating that they are functionally distinct from their non-adaptive
264 counterparts.

265 To assess whether CD49a^{+}KIR^{+}CD56^{bright}CD16^{-} blood NK cells segregate
266 further at the transcriptome level, we analyzed differentially expressed genes between
267 CD49a^{+}KIR^{+}CD56^{bright}CD16^{-} NK cells and CD49a^{-}KIR^{-}CD56^{bright}CD16^{-} NK cells. A
268 total of 351 genes were differentially expressed (padj<0.01, log2FC>1) and clearly
269 segregated both subsets (Fig. 6a). Based on high protein expression of CD49a, pan-
270 KIR, NKG2C, CD8, and lower expression of NKp80 and CD45RA (Fig. 1e, f and Fig.
271 5d, e), CD49a^{+}KIR^{+}CD56^{bright}CD16^{-} blood NK resembled cells to some extent
272 adaptive-like trNK cells in the lung. In order to identify similarities also at
273 transcriptome level, we next compared genes that were differentially expressed in

274 CD49a^{+}KIR^{+}CD56^{bright}CD16^{-} compared to CD49a^{-}KIR^{-}CD56^{bright}CD16^{-} NK cells in
275 peripheral blood with genes that were differentially expressed between non-adaptive
276 trNK cells (defined as CD69^{+}CD49a^{+}CD103^{+}NKG2A^{+}NKG2C^{-}CD16^{-} NK cells) and
277 non-tissue-resident CD69^{-}CD56^{bright}CD16^{-} NK cells in lung (Fig. 6b).
278 CD49a^{+}KIR^{+}CD56^{bright}CD16^{-} blood NK cells shared 73 DEGs with non-adaptive trNK
279 cells in lung, including high expression of *ITGA1* (CD49a), *ZNF683* (Hobit), *PRDM1*
280 (Blimp-1), *CCL5*, *PIK3R1*, *PLA2G16*, *ATXN1*, as well as lower expression of *SELL*
281 (CD62L), *GPR183*, *IL18R1*, *IL18RAP*, *SOX4*, *RAMP1*, and *IFITM3* (Fig. 6b). All of
282 these genes have also been shown to be differentially expressed in trNK cells in the
283 bone marrow and/or CD8^{+} T_{RM} cells in lung[35,36]. It should however be noted that other
284 core-genes associated with tissue-resident lymphocytes (e.g. *S1PR1*, *S1PR5*, *CXCR6*,
285 *ITGAE*, *RGS1*, *KLF2*, *KLF3*, and *RIPOR2*) were not differentially expressed between
286 CD49a^{+}KIR^{+}CD56^{bright}CD16^{-} and CD49a^{-}KIR^{-}CD56^{bright}CD16^{-}NK cells, indicating
287 that they only partially have a tissue-resident phenotype.

288 In addition to differentially expressing genes associated with tissue-residency,
289 CD49a^{+}KIR^{+}CD56^{bright}CD16^{-} blood NK cells shared differentially expressed genes
290 with adaptive-like trNK cells in lung (Fig. 6c) and/or adaptive CD56^{dim}CD16^{+} NK cells
291 in peripheral blood[8,29], including increased expression of *KIRs*, *KLRC2*, *GZMH*,
292 *ITGAD*, *CCL5*, *IL32*, *ZBTB38*, *CD3E*, *ARID5B*, *MCOLN2*, and *CD52,* and decreased
293 expression of *KLRB1*, *FCER1G*, *IL18RAP*, *IL2RB2*, *TLE1*, *AREG*, and *KLRF1* (Fig.
294 6a, c, Supplementary Fig. 3).

295 Taken together, CD49a^{+}KIR^{+}CD56^{bright}CD16^{-} NK cells in the blood share traits
296 with both non-adaptive lung trNK cells, adaptive-like lung trNK cells, and adaptive-
297 like CD56^{dim} blood NK cells.

298

299 *Increased metabolic modifications in adaptive-like CD49a^{+}NKG2C^{+}CD56^{bright}CD16^{-}*
300 *blood and lung NK cells*

301 Next, we sought to identify whether differential gene expression in
302 CD49a^{+}NKG2C^{+}CD56^{bright}CD16^{-} NK cells is consistent with distinct pathways specific
303 for this adaptive-like lung NK cell subset. Indeed, hallmark gene set enrichment
304 analysis (GSEA) of CD49a^{+}NKG2C^{+}CD56^{bright}CD16^{-} blood NK cells revealed a strong
305 enrichment for pathways associated with cell cycle arrest and DNA repair, including
306 'G2M checkpoint pathway', 'E2F targets', 'bile acid metabolism', 'UV response', and,
307 although not significant, the 'reactive oxygen species (ROS) pathway' (Fig. 6d,
308 Supplementary Fig. 4a). In adaptive-like lung trNK cells, only the ROS pathway was
309 significantly enriched, with five of the relevant core genes identical both in blood and
310 lung adaptive-like NK cells (i.e. *SOD1*, *SOD2*, *FTL*, *TXN* and *NDUFB4*) (Fig. 6e). Most
311 significantly downregulated gene set pathways in adaptive-like
312 CD49a^{+}NKG2C^{+}CD56^{bright}CD16^{-} NK cells were shared between peripheral blood and
313 lung, including pathways involved in 'IL6 JAK STAT3 signaling', 'TNFA signaling
314 via NFKB', 'IL2 STAT5 signaling', 'TGF beta signaling' and 'inflammatory response'
315 (Fig. 6f, g, Supplementary Fig. 4b, c). In addition to the above-mentioned pathways
316 involved in metabolic modifications, several distinct genes have been shown to be
317 associated to oxidative stress in cytokine-stimulated CD8^{+} T and NK cells[37-39]. Indeed,
318 gene expression levels for *TXN1*, *PRDX1*, and *SOD1* were higher in
319 CD49a^{+}KIR^{+}NKG2C^{+} CD56^{bright}CD16^{-} NK cells in both peripheral blood and lung as
320 compared to the non-adaptive counterpart (Supplementary Fig. 4d). However, while
321 *DUSP1* and *TXNIP*[39] were downregulated in adaptive-like lung trNK cells
322 (Supplementary Fig. 4e), no changes were observed in adaptive-like
323 CD49a^{+}CD56^{bright}CD16^{-} NK cells in healthy blood (Supplementary Fig. 4e).

324 Together, these results indicate modifications in the cellular metabolism in
325 adaptive-like CD49a^{+}KIR^{+}NKG2C^{+}CD56^{bright}CD16^{-} NK cells in blood and lung,
326 potentially caused by cytokine-induced stimulation and/or mitophagy during the
327 contraction-to-memory transition as discussed previously for murine memory NK
328 cells[40] and antigen-specific CD8^{+} T cells[41], respectively.

329 **Discussion**

330 Distinct subsets of putative human adaptive-like NK cells have been described
331 within the CD56^{dim}CD16^{+} subset in peripheral blood[5,6,8,10,42] and the CD56^{bright}CD16^{-}
332 subset in liver[7]. Here, we identified and characterized a yet unexplored and unique
333 subset of adaptive-like KIR^{+}NKG2C^{+}CD56^{bright}CD16^{-} NK cells in the human lung and
334 healthy human blood (Fig. 7). The lung adaptive-like NK cells displayed a tissue-
335 residency phenotype as indicated by co-expression of CD69, CD49a and CD103. Lung
336 adaptive-like trNK cells shared several phenotypic features with other adaptive-like NK
337 cell subsets both in blood and/or liver, including high expression of CD49a (liver),
338 CD69 (liver), CD2 (blood) and lack or lower expression of CD57 (liver), CD45RA
339 (liver) and perforin (liver), as well as low expression of FcεR1γ and Siglec-7 (blood)[5,7-
340 10,24,42,43]. However, lung adaptive-like NK cells segregate from their counterpart in the
341 liver by high expression of Eomes and CD103 and from those in blood by lack of CD57
342 and a CD56^{bright}CD16^{-} phenotype. Transcriptome analysis revealed shared core genes
343 in lung adaptive-like trNK cells and blood CD56^{dim}CD16^{+} adaptive-like NK cells,
344 underlining common features between the two subsets. Intriguingly, lung adaptive-like
345 trNK cells were highly target cell-responsive, and the overall blood and lung NK cell
346 populations were hyperresponsive in donors with expansions of adaptive-like trNK
347 cells in the lung. These findings indicate *in vivo* priming, which, however, did not
348 correlate with presence of tumor, HCMV serostatus, infection, or clinical and
349 demographic parameters. In fact, we could identify
350 CD49a^{+}KIR^{+}NKG2C^{+}CD56^{bright}CD16^{-} NK cells also in the peripheral blood of healthy
351 donors. These cells shared core gene sets with adaptive-like NK cells subsets both in
352 blood and lung and, despite the lack of CD103, also with non-adaptive trNK cells,
353 indicating tissue imprinting. Recently, a minute subset of T_{EM} cells expressing a tissue

354 signature has been shown in peripheral blood[44]. These findings suggest re-entry of
355 tissue-resident memory-associated lymphocytes from tissue into circulation. However,
356 it is yet unknown whether precursors of conventional or adaptive-like human lung trNK
357 cells are seeding the tissue from the circulation or whether the pool of trNK cells is
358 mainly replenished by proliferation within the tissue. In mice, MCMV-specific $CD8^+$
359 T cells convert to $CD103^+$ T_{RM} cells, with small numbers of new T_{RM} cells deriving
360 from the circulation[45], and memory inflation is required for retention of $CD8^+$ T_{RM} cells
361 in the lungs after intranasal vaccination with MCMV[46]. This indicates a dynamic
362 retention of T_{RM} cells by a persistent infection. In self-limiting viral infections of the
363 respiratory tract, conventional epitopes induce $CD8^+$ T_{RM} cells that wane over time[47].
364 It remains to be determined whether virus-dependent expansion and maintenance of
365 T_{RM} cells is analogous in adaptive-like trNK cells in the lung. Our data indicate,
366 however, that T_{RM} cells and adaptive-like NK cells differ in their recruitment to the
367 lung, with T_{RM} cells being dependent on CXCR6[48] while
368 $CD49a^+KIR^+NKG2C^+CD56^{bright}CD16^-$ blood NK cells lacked CXCR6 but expressed
369 high levels of CXCR3.

370 Since we showed that adaptive-like lung trNK cells were hyperresponsive, they
371 might be clinically relevant, e.g. in the defense against malignant target cells. Lung
372 $CD8^+$ T_{RM} cells have previously been shown to be able to control tumor growth and to
373 be essential for anti-cancer vaccination in mice and also correlated with increased
374 survival in lung cancer patients[49]. In addition to strong target cell-responsiveness, we
375 observed increased gene expression levels of *GZMH* and *CCL5* in adaptive-like lung
376 and blood NK cells, respectively. An antiviral activity has been proposed for granzyme
377 H[50,51], however, a direct association of this effector molecule with adaptive-like NK
378 cells remains to be determined. CCL5 and XCL1, chemokines upregulated in adaptive-

379 like lung trNK cells, were predominantly produced by mouse Ly49H$^+$ NK cells upon
380 stimulation with MCMV-derived m157 protein[52], and CCL5 has been shown to be
381 specifically expressed by CD8$^+$ memory T_{EM} cells[53]. Thus, adaptive-like
382 CD49a$^+$KIR$^+$NKG2C$^+$CD56^{bright}CD16$^-$ blood and lung NK cells share also functional
383 characteristics with other memory lymphocyte subsets.

384 Adaptive-like lung trNK cell expansions were rarely observed in donors with
385 adaptive-like CD56^{dim}CD16$^+$ NK cell expansions, indicating that these two distinct
386 subsets have distinct developmental cues. Indeed, even in the rare cases where we could
387 detect expansions of both adaptive-like lung trNK cells and CD56^{dim}CD16$^+$ NK cells
388 in the same individual, these populations displayed distinct KIR repertoires.
389 Furthermore, expansions of adaptive-like lung trNK cells were detected in HCMV-
390 seronegative individuals (Supplementary Fig. 2e, f), while expansions of adaptive-like
391 CD56^{dim}CD16$^+$ NK cells were restricted to HCMV-seropositive individuals
392 (Supplementary Fig. 2e)[5,42]. It thus remains possible that other viral infections could
393 drive the expansion of adaptive-like trNK cells, as has previously been suggested for
394 the generation of cytokine-induced memory NK cells after influenza virus infection in
395 humans[54] and mice[15]. Taken together, our data support a model where adaptive-like
396 trNK cells and adaptive-like CD56^{dim}CD16$^+$ NK cells develop independently from each
397 other, possibly due to distinct environmental requirements for their expansion.

398 Our results revealed accumulation of gene sets predictive of adaptive-like lung
399 trNK cells controlling dysfunctional mitochondria and ROS. In mice, MCMV-specific
400 Ly49H$^+$ NK cells have been shown to control the removal of dysfunctional
401 mitochondria via mitophagy, allowing the formation of a stable reservoir of memory
402 NK cells[40]. Human adaptive-like CD56^{dim}CD16$^+$ NK cells displayed an elevated
403 mitochondrial function and quality[29], and mitochondrial fitness was crucial for the

404 generation of $CD8^+$ T cell memory[55]. Hence, metabolic adaptations might be a common
405 characteristic between different lines of adaptive-like cytotoxic lymphocytes.
406 Together, our data reveal the presence of a yet unexplored and distinct adaptive-
407 like trNK cell subset in the human lung, indicating that adaptive-like NK cells are not
408 confined to peripheral blood and/or liver. Expansions of adaptive-like trNK cells in the
409 lung are mostly accompanied by the presence of
410 $CD49a^+KIR^+NKG2C^+CD56^{bright}CD16^-$ NK cells in peripheral blood, enabling the non-
411 invasive identification of potential donors with adaptive-like lung trNK cell expansions.
412 Since adaptive-like trNK cells were strongly target cell-responsive, these cells might
413 be clinically relevant in the defense of lung cancer and/or respiratory viral infections.

414 **Material and methods**

415

416 *Lung patients and healthy blood*

417 A total of 103 patients undergoing lobectomy for suspected lung cancer were included
418 in this study. None of the patients received preoperative chemotherapy and/or
419 radiotherapy. Patients with records of strong immunosuppressive medication and/or
420 hematological malignancy were excluded from the study. Clinical and demographic
421 details are summarized in Table 1. Furthermore, healthy blood was collected from
422 regular blood donors. The regional review board in Stockholm approved the study, and
423 all donors gave informed written consent prior to collection of samples.

424

425 *Processing of tissue specimens and peripheral blood*

426 Lung tissue was processed as previously described[20]. Briefly, a small part of
427 macroscopically tumor-free human lung tissue from each patient was transferred into
428 ice-cold Krebs-Henseleit buffer and stored on ice for less than 18 h until further
429 processing. The tissue was digested using collagenase II (0.25 mg/ml, Sigma-Aldrich)
430 and DNase (0.2 mg/ml, Roche), filtered and washed in complete RPMI 1640 medium
431 (Thermo Scientific) supplemented with 10% FCS (Thermo Scientific), 1 mM L-
432 glutamine (Invitrogen), 100 U/ml penicillin, and 50 µg/ml streptomycin (R10 medium).
433 Finally, mononuclear cells from the lung cell suspensions and peripheral blood were
434 isolated by density gradient centrifugation (Lymphoprep).

435

436 *RNA-sequencing and RNAseq data analysis*

437 RNA of sorted NK cell subsets from blood and lung were sequenced and analyzed as
438 described previously[25]. Briefly, RNAseq was performed using a modified version of

439 the SMART-Seq2 protocol[56]. For analysis of lung adaptive-like NK cells, live
440 NKG2C^{+}KIR^{+}CD3^{-}CD14^{-}CD19^{-}CD56^{+}CD16^{-} NK cells were sorted from two donors
441 and were compared to previously published data on CD69^{+}CD49a^{+}CD103^{-} and
442 CD69^{+}CD49a^{+}CD103^{+} NKG2A^{+}CD16^{-} trNK cells (GSE130379)[25]. For analysis of
443 KIR^{+}CD49a^{+} CD56^{bright}CD16^{-} NK cells, we sorted KIR^{+}CD49a^{+} and KIR^{-}CD49a^{-} live
444 CD14^{-}CD19^{-}CD3^{-}CD56^{bright}CD16^{-} NK cells from cryopreserved PBMCs from 4
445 donors. Duplicates of 100 cells from each population from two individual donors were
446 sorted into 4.2ul of lysis buffer (0.2% Triton X-100, 2.5uM oligo-dT (5′-
447 AAGCAGTGGTATCAACGCAGAGTACT30VN-3′), 2.5mM dNTP, RNAse
448 Inhibitor (Takara), and ERCC RNA spike in controls (Ambion)) in a 96-well V-bottom
449 PCR plate (Thermo Fisher). Sorted cells were then frozen and stored at -80°C until they
450 could be processed. Subsequent steps were performed following the standard SMART-
451 Seq2 protocol with 22 cycles of cDNA amplification and sample quality was
452 determined using a bioanalyzer (Agilent, High Sensitivity DNA chip). 5ng of amplified
453 cDNA was taken for tagmentation using a customized in-house protocol[57] and Nextera
454 XT primers. Pooled samples were sequenced on a HiSeq2500 on high output mode with
455 paired 2x125bp reads.
456
457 *Transcriptome analysis*
458 Following sequencing and demultiplexing, read pairs were trimmed from Illumina
459 adapters using cutadapt (version 1.14)[58], and UrQt was used to trim all bases with a
460 phred quality score below 20[59]. Read pairs were subsequently aligned to the protein
461 coding sequences of the human transcriptome (gencode.v26.pc_transcripts.fa) using
462 Salmon (version 0.8.2)[60], and gene annotation using gencode.v26.annotation.gtf.
463 DeSeq2[61] was used to analyze RNA-seq data in R studio version 1.20. Briefly, raw

464 count values were used as input into deSeq2, and variance stabilizing transformation
465 was used to transform data. Data were batch- and patient corrected using Limma[62]. A
466 cut-off of >100 counts across the samples was used to filter out low expressed genes.
467 Genes with an adjusted p-value<0.05 and a log2-fold change greater than 1 were
468 considered as differentially expressed between paired samples. Similarly, previously
469 published data sets on adaptive-like NKG2C^{+}CD57^{+}CD56^{dim}CD16^{+} NK cells and
470 conventional NKG2C^{-}CD57^{+}CD56^{dim} NK cells (GSE117614)[29] were analyzed using
471 deSeq2 to identify differentially expressed genes. Heatmaps of gene expression were
472 generated using Pheatmap in R and show the z-score for differentially expressed genes
473 (as determined above in deSeq2) for all donors and replicates.
474
475 *Flow cytometry*
476 Antibodies and clones reactive against the following proteins were used: CD2 (TS1/8,
477 BV421 or Pacific Blue, Biolegend), CD3 (UCHT1, PE-Cy5, Beckman Coulter), CD8
478 (RPA-T8, Brilliant Violet 570, Biolegend, or RPA-8, BUV395 or SK1, BUV737, BD
479 Biosciences), CD14 (MφP9, Horizon V500, BD Biosciences), CD16 (3G8, Brilliant
480 Violet 570 or Brilliant Violet 711, or Brilliant Violet 785, Biolegend), CD19 (HIB19,
481 Horizon V500, BD Biosciences), CD38 (HIT2, Brilliant Violet 711 or BUV661, BD
482 Biosciences), CD45 (HI30, Alexa Fluor 700, Biolegend, or BUV805, BD Biosciences),
483 CD45RA (HI100, Brilliant Violet 785, Biolegend), CD49a (TS2A, AlexaFluor 647,
484 Biolegend, or HI30, BUV615, or 8R84, Brilliant Violet 421, BD Biosciences), CD56
485 (N901, ECD, Beckman Coulter, or HCD56, Brilliant Violet 711, Biolegend, or
486 NCAM16.2, PE-Cy7, or BUV563, BD Biosciences), CD57 (TB01, purified,
487 eBioscience, or HNK-1, Brilliant Violet 605, Biolegend), CD103 (APC, B-Ly7,
488 eBioscience, or biotin, 2G5, Beckman Coulter, or Ber-ACT8, Brilliant Violet 711,

489 BUV395, BD Biosciences, or Ber-ACT8, PE-Cy-7, Biolegend), KIR2DL1
490 (FAB1844F, biotin, R&D Systems), KIR2DL3 (180701, FITC, R&D Systems),
491 KIR3DL1 (DX9, Brilliant Violet 421, Biolegend), KIR3DL2 (DX-31, Brilliant Violet
492 711, Biolegend), KIR2DL2/S2/L3 (GL183, PE-Cy5.5, Beckman Coulter),
493 KIR2DL1/S1 (EB6, PE-Cy5.5 or PE-Cy7, Beckman Coulter), NKG2A (Z1991.10,
494 APC-A780, or PE, Beckman Coulter, or 131411, BUV395, BD Biosciences), NKG2C
495 (134591, Alexa-Fluor 488 or PE, R&D Systems), CD69 (TP1.55.3, ECD, Beckman
496 Coulter, or FN50, PE-CF594, BD Biosciences, or FN50, Brilliant Violet 786,
497 Biolegend), CD127 (Brilliant Violet 421, HIL-7R-M21, BD Biosciences or PE-Cy7,
498 R34.34, Beckman Coulter), CD161 (HP3-3G10, Brilliant Violet 605 or APC/Fire 750,
499 Biolegend), CXCR3 (Alexa Fluor 647, G025H7, Biolegend), CXCR6 (K041E5,
500 Brilliant Violet 421, Biolegend), CD85j/ILT2 (HP-F1, Super Bright 436, Invitrogen),
501 NKp80 (5D12, PE, BD Biosciences, or 4A4.D10, PE-Vio770, Miltenyi), Siglec-7 (5-
502 386, Alexa Fluor 488, Bio-Rad), TIM-3 (7D3, Brilliant Violet 711, BD Biosciences).
503 After two washes, cells were stained with streptavidin Qdot 605 or Qdot 585 (both
504 Invitrogen), anti-mouse IgM (II/41, eFluor 650NC, eBioscience) and Live/Dead Aqua
505 (Invitrogen). After surface staining, peripheral blood mononuclear cells (PBMC) were
506 fixed and permeabilized using FoxP3/Transcription Factor staining kit (eBioscience).
507 For intracellular staining the following antibodies were used: Eomes (WF1928, FITC,
508 eBioscience), FcεR1γ (polyclonal, FITC, Merck), granzyme B (GB11, BB790, BD
509 Biosciences), Ki67 (B56, Alexa Fluor 700, BD Biosciences), perforin (dG9, BB755,
510 BD Biosciences, or B-D48, Brilliant Violet 421, Biolegend), T-bet (4B10, Brilliant
511 Violet 421, BD Biosciences), and TNF (MAb11, Brilliant Violet 421, Biolegend, or
512 Brilliant Violet 650, BD Biosciences). Purified NKG2C (134591, R&D Systems) was

513 biotinylated using a Fluoreporter Mini-biotin XX protein labeling kit (Life
514 Technologies) and detected using streptavidin-Qdot 585, 605 or 655 (Invitrogen).
515 Samples were analyzed on a BD LSR Fortessa equipped with four lasers (BD
516 Biosciences) or a BD FACSymphony A5 equipped with five lasers (BD Biosciences),
517 and data were analyzed using FlowJo version 9.5.2 and version 10.6.1 (Tree Star Inc).
518 UMAPs were constructed in FlowJo 10.6.1 using the UMAP plugin. UMAP
519 coordinates and protein expression data were subsequently exported from FlowJo, and
520 protein expression for each parameter was normalized to a value between 0 and 100.
521 UMAP plots were made in R using ggplot, and color scale show log2(normalized
522 protein expression +1).
523 For sorting of NK cells from lung and peripheral blood for RNA sequencing,
524 thawed cryopreserved mononuclear cells were stained with anti-human CD57 (NK-1,
525 FITC, BD Biosciences), CD16 (3G2, Pacific Blue, BD Biosciences), CD14 (MφP9,
526 Horizon V500, BD Biosciences), CD19 (HIB19, Horizon V500, BD Biosciences),
527 CD103 (Ber-ACT8, Brilliant Violet 711, BD Biosciences), CD49a (TS2/7, Alexa Fluor
528 647, Biolegend), CD45 (HI30, A700, Biolegend), CD8 (RPA-T8, APC/Cy7, BD
529 Biosciences), NKG2A (Z199.10, PE, Beckman Coulter), CD69 (TP1.55.3, ECD,
530 Beckman Coulter), CD3 (UCHT1, PE/Cy5, Beckman Coulter), KIR2DL1/S1 (EB6,
531 PE/Cy5.5, Beckman Coulter), KIR2DL2/3/S2 (GL183, PE/Cy5.5, Beckman Coulter,),
532 NKG2C (134591, biotin, R&D Systems, custom conjugate), CD56 (NCAM16.1,
533 PE/Cy7, BD Biosciences), streptavidin Qdot655 (Invitrogen), and Live/Dead Aqua
534 (Invitrogen).
535
536 *DNA isolation and KIR/HLA-ligand genotyping*

537 Genomic DNA was isolated using a DNeasy Blood & Tissue Kit (Qiagen) from 100 µl
538 of whole blood. KIR genotyping and KIR ligand-determination were performed using
539 PCR-SSP technology with a *KIR* typing kit and a *KIR HLA* ligand kit (both Olerup-
540 SSP) according to the manufacturer's instructions.
541
542 *CMV IgG ELISA*
543 Concentrations of anti-CMV IgG relative to a standard curve and internal negative and
544 positive control were determined by ELISA (Abcam, UK) and read in a microplate
545 spectrophotometer (Bio-Rad xMark) at 450nm with a 620nm reference wavelength.
546
547 *Activation assay*
548 Degranulation and TNF production of fresh blood and lung NK cells were assessed as
549 previously described[20,22]. In brief, fresh lung and blood mononuclear cells were
550 resuspended in R10 medium and rested for 15 to 18 hours at 37°C. Subsequently, the
551 cells were co-cultured in R10 medium alone or in presence of K562 cells for 2 hours in
552 the presence of anti-human CD107a (FITC or Brilliant Violet 421, H4A3, BD
553 Biosciences, San Jose, Calif.).
554
555 *Statistics*
556 GraphPad Prism 6 and 7 (GraphPad Software) was used for statistical analysis. For
557 each analysis, measurements were taken from distinct samples. The statistical method
558 used is indicated in each figure legend.

559 **Data Availability**

560 The dataset generated for this study can be found in the Gene Expression Omnibus with
561 accession no. xxxx (data will be deposited and made available before publication).

562

563 **Author contribution**

564 Conceptualization: N.M., H.G.L., Ja.M.; Methodology: N.M., Ja.M.; Investigation:
565 N.M., M.S., Je.M., J.H., E.K., M.B., S.N., J.N.W.; Resources: M.A.-A.; Writing –
566 original draft: N.M., Ja.M.; Writing – review and editing: N.M., Ja.M., H.G.L;
567 Visualization: N.M., Ja.M.; Funding acquisition: N.M., Ja.M., H.G.L.

568

569 **Acknowledgements**

570 The authors acknowledge support from the National Genomics Infrastructure in
571 Stockholm funded by Science for Life Laboratory, the Knut and Alice Wallenberg
572 Foundation, the Swedish Research Council, and SNIC/Uppsala Multidisciplinary
573 Center for Advanced Computational Science for assistance with massively parallel
574 sequencing and access to the UPPMAX computational infrastructure. The authors also
575 acknowledge the MedH Core Flow Cytometry Facility (Karolinska Institutet),
576 supported by Karolinska Institutet and Region Stockholm, for providing cell-sorting
577 services. Furthermore, the authors want to thank all donors for participating in the study
578 and A.-C. Orre, V. Jackson, and S. Hylander for administrative and clinical help as well
579 as E. Yilmaz for assistance in the laboratory. This work was supported by the Swedish
580 Research Council, the Strategic Research Foundation, the Swedish Foundation for
581 Strategic Research, the Swedish Cancer Society, Sweden's Innovation Agency, the Eva
582 and Oscar Ahréns Research Foundation, the Åke Wiberg Foundation and the
583 Tornspiran Foundation.

584

585 **Disclosures**

586 The authors have no financial or other conflicts of interest.

587 **Figure legends**

588 **Figure 1: Adaptive-like KIR$^+$NKG2C$^+$ NK cells exist in the CD56^{bright}CD16$^-$ NK**
589 **cell subset in the human lung. (a)** Representative overlay displaying pan-KIR and
590 NKG2C expression on CD56^{dim}CD16$^+$ NK cells in matched blood (black contour) and
591 lung (orange). **(b)** Representative dot plots displaying pan-KIR and NKG2C expression
592 on CD56^{bright}CD16$^-$ NK cells in the lungs of three different donors. **(c)** Summary of
593 data showing the frequencies of KIR$^+$NKG2C$^+$ NK cells in CD56^{dim}CD16$^+$ and
594 CD56^{bright}CD16$^-$ NK cells in blood and lung (n = 77). Friedman test, Dunn's multiple
595 comparisons test. ***p<0.001, ****p<0.0001. **(d)** UMAP analysis of CD56^{bright}CD16$^-$
596 lung NK cells from four donors with 2,000 events/donor (942 events in one of the
597 donors). UMAPs were constructed using expression of Siglec-7, CD8, CD2, CD57,
598 CD161, NKG2C, CD56, CD45RA, NKG2A and NKp80. Color scale shows
599 log2(normalized expression + 1). **(e)** Representative histograms and **(f)** summary of
600 data showing surface expression of NKG2A (n = 27), CD57 (n = 27), Siglec-7 (n = 7),
601 CD161 (n = 12), CD2 (n = 5), ILT2 (n = 6), CD8 (n = 20), NKp80 (n = 6), CD45RA (n
602 = 5), and intracellular expression of FcεR1γ (n = 4), Eomes (n = 7) and T-bet (n = 6) in
603 KIR$^+$NKG2C$^+$ NK cells in CD56^{dim}CD16$^+$ blood (grey) and lung (orange) NK cells and
604 CD56^{bright}CD16$^-$ lung NK cells (blue). Friedman test, Dunn's multiple comparisons
605 test. *p<0.05, **p<0.01, ***p<0.001, ****p<0.0001.

606

607 **Figure 2: Adaptive-like CD56^{bright}CD16$^-$ lung NK cells are tissue-resident. (a)**
608 Overlay of UMAPs from data from Figure 1, showing the position of NKG2C$^+$ (blue)
609 and NKG2C$^-$ (grey) populations among CD56^{bright}CD16$^-$ NK cells. **(b)** Expression of
610 the tissue-residency markers CD69, CD49a, and CD103 within the UMAP of
611 CD56^{bright}CD16$^-$ lung NK cells. **(c)** Representative histograms and **(d)** summary of data

612 showing the expression of the tissue-residency markers CD69 (n = 23), CD49a (n= 21)
613 and CD103 (n = 21) on $CD56^{dim}CD16^{+}$ blood (grey) and lung (orange) NK cells and
614 $CD56^{bright}CD16^{-}$ lung NK cells (blue), respectively. Friedman test, Dunn's multiple
615 comparisons test. *p<0.05, **p<0.01, ***p<0.001, ****p<0.0001. **(e)** Heatmap
616 showing 102 differentially expressed genes between $KIR^{+}NKG2C^{+}$ trNK cells and
617 $KIR^{-}NKG2C^{-}$ trNK cells in the human lung. Differentially expressed genes shared with
618 $CD57^{+}NKG2C^{+}CD56^{dim}CD16^{+}$ adaptive-like NK cells in blood (from GSE117614) are
619 highlighted in red. **(f)** Log2 fold-change for $NKG2C^{-}$ trNK cells vs $KIR^{+}NKG2C^{+}$ trNK
620 cells in lung against log2 fold change for $CD57^{+}$NKG2C- vs $CD57^{+}NKG2C^{+}$ $CD56^{dim}$
621 NK cells in blood. Data for $CD56^{dim}$ NK cells in peripheral blood are from GSE117614
622 [29]. **(g-i)** Single KIR expression analysis on $CD56^{dim}CD16^{+}$ NK cells from peripheral
623 blood (red), $CD49a^{-}CD103^{-}CD56^{dim}CD16^{+}$ or $CD103^{-}CD56^{dim}CD16^{+}$ (black) and
624 $CD49a^{+}CD103^{+}CD56^{bright}CD16^{-}$ or $CD103^{+}CD56^{bright}CD16^{-}$ (blue) NK cells in
625 matched lung of three different donors. Educating KIR are highlighted in red. **(g)** Donor
626 with expansions of self-KIR^{+} NK cells both in the $CD56^{dim}CD16^{+}$ subset in blood and
627 lung and in the $CD56^{bright}CD16^{-}$ NK cell subset in the lung. **(h)** Donor with an
628 expansion of self-KIR^{+} NK cells exclusively in the $CD56^{bright}CD16^{-}$ NK cell subset in
629 the lung. **(i)** Donor with expansions of self-KIR^{+} NK cells both in the $CD56^{dim}CD16^{+}$
630 and $CD56^{bright}CD16^{-}$ subsets in blood and lung, respectively.
631
632 **Figure 3: Adaptive-like lung trNK cells are highly functional. (a)** Gene expression
633 levels (counts per million reads) for selected genes associated with functional capacity
634 are shown for $CD49a^{+}KIR^{-}NKG2C^{-}$ and $CD49a^{+}KIR^{+}NKG2C^{+}$ lung trNK cells (clear
635 circles: $CD49a^{+}CD103^{-}$ NK cells, filled circles: $CD49a^{+}CD103^{+}$ NK cells). Mean ±
636 SEM is shown. **(b)** Representative histograms and **(c)** summary of data displaying

637 expression of perforin and granzyme B (GzmB) (n = 4) in $CD56^{dim}CD16^{+}$ and in
638 $CD49a^{-}KIR^{-}NKG2C^{-}$ as well as $CD49a^{+}KIR^{+}NKG2C^{+}$ NK cells within the
639 $CD56^{bright}CD16^{-}$ NK cell subset, respectively, in human lung ex vivo. $CD14^{-}CD19^{-}$
640 $CD3^{-}CD45^{+}CD127^{+}CD161^{+}$ cells were gated as controls in (b). Friedman test, Dunn's
641 multiple comparisons test. *p<0.05. **(d)** Representative dot plots showing expression
642 of CD107a and CD49a on $KIR^{-}NKG2C^{-}$ and $KIR^{+}NKG2C^{+}$ NK cells in a donor without
643 (upper panel) and with (lower panel) expansion of $CD49a^{+}KIR^{+}NKG2C^{+}$ NK cells in
644 the lung (expression KIR and NKG2C are displayed in the left panel for each of the
645 two donors). **(e)** Summary of data showing the frequency of K562 target cell-induced
646 $CD107a^{+}$ (left) and TNF^{+} (right) NK cell subsets from donors with NK cell expansions
647 in the human lung. Responses by unstimulated controls were subtracted from
648 stimulated cells (n = 3). Mean ± SD is shown. **(f)** Representative dot plots showing
649 expression of CD107a and TNF vs CD103 on $CD49a^{+}KIR^{-}NKG2C^{-}$ (upper panel) or
650 $CD49a^{+}KIR^{+}NKG2C^{+}$ (lower panel) bulk NK cells in a donor with an expansion of
651 $CD49a^{+}KIR^{+}NKG2C^{+}$ NK cells in the lung. **(g, h)** Summary of data showing the
652 frequencies of **(g)** $CD107a^{+}$ and **(h)** TNF^{+} NK cells in blood NK cells and in subsets of
653 lung NK cells ($CD49a^{-}CD103^{-}$, expressing either CD49a or CD103, or
654 $CD49a^{+}CD103^{+}$) from donors without (left panels, n = 5 for CD107a, n= 3 for TNF) or
655 with (right panels, n = 4) expansions of $KIR^{+}NKG2C^{+}$ trNK cells in the lung. Responses
656 by unstimulated controls were subtracted from stimulated cells. (g, h) Violin plots with
657 quartiles and median are shown. Friedman test, Dunn's multiple comparisons test.
658 *p<0.05.
659
660 **Figure 4: Expansions of adaptive-like trNK cell in the lung indicate presence of**
661 **adaptive-like $CD49a^{+}KIR^{+}NKG2C^{+}$ NK cells in matched blood (a)** Representative

662 dot plots displaying expression of CD49a and NKG2C on NK cells in lung and matched
663 peripheral blood. **(b)** Summary of data of frequencies of CD49a^{+}KIR^{+}NKG2C^{+} NK
664 cells of the CD16^{-} NK cell subset and of CD49a^{-}KIR^{+}NKG2C^{+} cells in the CD16^{+} NK
665 cell subset in lung and peripheral blood. Adaptive-like NK cell "expansions" were
666 identified as outliers (filled circles) using the Robust regression and Outlier removal
667 (ROUT) method (ROUT coefficent Q=1). Error bars show the median with
668 interquartile range (n = 86). Median with interquartile range is shown. **(c)** Euler diagram
669 indicating overlaps and relationships between CD16^{-}CD49a^{+}KIR^{+}NKG2C^{+} and
670 CD16^{+}CD49a^{-}KIR^{+}NKG2C^{+} NK cell expansions in peripheral blood and lung. The
671 number of individuals with overlaps between the subsets and compartments are
672 indicated in the circles. **(d)** Representative overlays and **(e)** summary of data showing
673 phenotypic differences between CD49a^{+}KIR^{+}NKG2C^{+} (blue) and CD49a^{-}KIR^{-}
674 NKG2C^{-} (grey) NK cells within the CD56^{bright}CD16^{-} NK cell subset in blood. (NKG2A,
675 n=6; CD57, n=5; CD69, n=6; CD103, n=6; CD127, n=3; CD161, n=4). Violin plots
676 with quartiles and median are shown.
677
678 **Figure 5: Expansions of CD49a^{+}KIR^{+}NKG2C^{+} CD56^{bright}CD16^{-} NK cells in**
679 **healthy blood donors. (a)** Representative dot plot (left plot) and overlay (right plot)
680 showing expression of KIR and NKG2C (left plot), and CD49a on KIR^{+}NKG2C^{+} NK
681 cells (blue) versus KIR^{-}NKG2C^{-} NK cells (grey) (right plot) within CD16^{-} blood NK
682 cells of healthy blood donors. **(b)** Identification of expansions (filled circles) of CD49a^{-}
683 KIR^{+}NKG2C^{+} within the CD56^{dim}CD16^{+} NK cell subset (21 outliers, 20%) and
684 CD49a^{+}KIR^{+}NKG2C^{+} cells within the CD56^{bright}CD16^{-} NK cell subset (17 outliers,
685 16%) via the ROUT method (see also Figure 4e). Error bars show the median with
686 interquartile range. (n=95). Median with interquartile range is shown. **(c)** Frequencies

687 of KIR^{+}NKG2C^{+} cells of CD49a^{-}CD16^{-} or CD49a^{+}CD16^{-} NK cells in healthy blood.
688 The respective maternal population comprised at least 45 cells (n=13). Wilcoxon
689 matched-pairs signed rank test. **p<0.005 **(d)** UMAPs based on CD56^{bright}CD16^{-} NK
690 cells from three donors with KIR^{+}NKG2C^{+}CD56^{bright}CD16^{-} NK cells. UMAPs were
691 constructed using expression of CXCR3, CD161, Ki67, NKG2C, CD103, TIGIT,
692 perforin, granzyme B, NKG2A, CD16, CD56, CD49a, CD38, CD8, CXCR6, CD4,
693 CD57, CD45RA, NKp80, CD69, GL183/EB6 (KIR), and CD127. Color scale indicates
694 log2(normalized protein expression +1) for each parameter. **(e)** Summary of protein
695 expression on CD49a^{+}KIR^{+}NKG2C^{+} NK cells from peripheral blood from healthy
696 donors. (CD69, n=11; CD103, n=7; CD57, n=11; NKG2A, n=11; CD127, n=7; CD161,
697 n=7; CD8, n=11; CD38, n=5; CD45RA, n=4; NKp80, n=5; TIM-3, n=5; CXCR3, n=4;
698 CXCR6, n=5; Ki67, n=5; perforin, n=7; granzyme B, n=5). Violin plots with quartiles
699 and median are shown. **(f)** Gene expression levels (counts per million reads) for selected
700 genes associated with functional capacity are shown for CD49a^{-}KIR^{-} and CD49a^{+}KIR^{+}
701 blood CD56^{bright}CD16^{-} NK cells. Mean ± SEM is shown.
702
703 **Figure 6: CD49a^{+}KIR^{+}NKG2C^{+}CD56^{bright}CD16^{-} NK cells in healthy blood donors**
704 **share traits with both trNK cells and with adaptive-like trNK cells. (a)** Heatmap
705 showing 138 differentially expressed genes (padj<0.001, log2FC>2) between
706 CD56^{bright}CD16^{-}CD49a^{-}KIR^{-} and CD56^{bright}CD16^{-}CD49a^{+}KIR^{+} NK cells in peripheral
707 blood from unrelated healthy donors (n=4). Genes shared with trNK cells in the lung
708 were highlighted in dark blue, shared with adaptive-like trNK cells in bright blue, and
709 genes shared with adaptive-like CD56^{dim}CD16^{+} NK cells in healthy blood in orange.
710 **(b)** Log2 fold-change for trNK cells vs CD56^{bright}CD16^{-} NK cells in lung against log2
711 fold-change for CD49a^{+}KIR^{+}CD56^{bright}CD16^{-} vs CD49a^{-}KIR^{-}CD56^{bright}CD16^{-} NK

712 cells in blood. **(c)** Log2 fold-change for $KIR^{+}NKG2C^{+}$ trNK cells vs $NKG2C^{-}$ trNK
713 cells in lung against log2 fold-change for $CD49a^{+}KIR^{+}CD56^{bright}CD16^{-}$ vs $CD49a^{-}KIR^{-}$
714 $CD56^{bright}CD16^{-}$ NK cells in blood. **(d)** GSEA from (a) showing significantly enriched
715 gene sets of adaptive-like NK cells in healthy blood. **(e)** Hallmark GSEA enrichment
716 plots for 'reactive oxygen species pathway' for $CD49a^{+}KIR^{+}NKG2C^{+}$ adaptive-like
717 NK cells in lung (left) and blood (right). Shared genes between lung and blood
718 enrichment plots are highlighted. Core gene sets are marked in red, and negative rank
719 metric scores in blue. **(f, g)** GSEA from (a) showing significantly enriched gene sets of
720 non-adaptive trNK cells in **(f)** lung and **(g)** blood. **(d, f, g)** Pathways which were unique
721 and not shared with the respective reference population are highlighted in blue, and
722 gene sets significantly enriched at a nominal p value <1% are highlighted in red.
723
724 **Figure 7: Overview adaptive-like NK cell subsets that can be identified in human**
725 **lung and/or peripheral blood.** Both unique and shared characteristics at protein and
726 transcriptome between adaptive-like lung trNK cells,
727 $CD49a^{+}KIR^{+}NKG2C^{+}CD56^{bright}CD16^{-}$ blood NK cells, and adaptive-like
728 $CD56^{dim}CD16^{+}$ blood NK cells are shown.

729 Table 1. Clinical and demographic details of the 103 patients included in the study.

730

	Non-smoker (n = 16)	**Current smoker** (n = 25)	**Ex-smoker** (n = 62)
Female / male	8 / 8	14 / 11	41 / 21
Age (y), mean ± SD	67 ± 13.4	67 ± 8.0	69 ± 7.1
FEV1/FVC (% of predicted) mean ± SD	100 ± 10.3	88 ± 13.7*	93 ± 14.9#
Pathology	***% (n)***	***% (n)***	***% (n)***
Non-malignant	6 (1)	4 (1)	2 (1)
Adenocarcinoma	44 (7)	52 (13)	76 (47)
Large cell carcinoma	0 (0)	12 (3)	3 (2)
Squamous cell carcinoma	6 (1)	16 (4)	5 (3)
Metastasis	0 (0)	4 (1)	3 (2)
Carcinoid	31 (5)	8 (2)	6 (4)
Adenosquamous carcinoma	6 (1)	0 (0)	3 (2)
Other§	6 (1)	4 (1)	2 (1)
Medication	***% (n)***	***% (n)***	***% (n)***
Inhaled corticosteroids	19 (3)	0 (0)	2 (1)
Statins	38 (6)	28 (7)	31 (19)
Systemic immunosuppression	0 (0)	4 (1)	5 (3)
Beta-agonists or anti-cholinergics	0 (0)	12 (3)	13 (8)
Inhaled corticosteroid and long-acting beta-agonist combination	0 (0)	8 (2)	6 (4)
Diagnoses affecting lung function	***% (n)***	***% (n)***	***% (n)***
Asthma	19 (3)	0 (0)	5 (3)
COPD	0 (0)	32 (8)	10 (6)
Other lung parenchyme disease	6 (1)	0 (0)	2 (1)

731 * n = 24

732 # n = 59

733 § = uncertain histopathological diagnosis, data missing, combined small cell carcinoma

734

735 **References**

736 1. Sun, J. C., Beilke, J. N. & Lanier, L. L. Adaptive immune features of natural
737 killer cells. *Nature* **457,** 557–561 (2009).
738 2. Cooper, M. A. *et al.* Cytokine-induced memory-like natural killer cells.
739 *Proceedings of the National Academy of Sciences of the United States of*
740 *America* **106,** 1915–1919 (2009).
741 3. O'Leary, J. G., Goodarzi, M., Drayton, D. L. & Andrian, von, U. H. T cell- and
742 B cell-independent adaptive immunity mediated by natural killer cells. *Nature*
743 *immunology* **7,** 507–516 (2006).
744 4. Paust, S. *et al.* Critical role for the chemokine receptor CXCR6 in NK cell-
745 mediated antigen-specific memory of haptens and viruses. *Nature immunology*
746 **11,** 1127–1135 (2010).
747 5. Guma, M. *et al.* Imprint of human cytomegalovirus infection on the NK cell
748 receptor repertoire. *Blood* **104,** 3664–3671 (2004).
749 6. Lopez-Vergès, S. *et al.* Expansion of a unique CD57^{+}NKG2Chi natural killer
750 cell subset during acute human cytomegalovirus infection. *Proceedings of the*
751 *National Academy of Sciences of the United States of America* **108,** 14725–
752 14732 (2011).
753 7. Marquardt, N. *et al.* Cutting Edge: Identification and Characterization of
754 Human Intrahepatic CD49a+ NK Cells. *J. Immunol.* **194,** 2467–2471 (2015).
755 8. Schlums, H. *et al.* Cytomegalovirus infection drives adaptive epigenetic
756 diversification of NK cells with altered signaling and effector function.
757 *Immunity* **42,** 443–456 (2015).
758 9. Lee, J. *et al.* Epigenetic modification and antibody-dependent expansion of
759 memory-like NK cells in human cytomegalovirus-infected individuals.
760 *Immunity* **42,** 431–442 (2015).
761 10. Béziat, V. *et al.* NK cell responses to cytomegalovirus infection lead to stable
762 imprints in the human KIR repertoire and involve activating KIRs. *Blood* **121,**
763 2678–2688 (2013).
764 11. Cerwenka, A. & Lanier, L. L. Natural killer cell memory in infection,
765 inflammation and cancer. *Nature reviews. Immunology* **16,** 112–123 (2016).
766 12. Kuijpers, T. W. *et al.* Human NK cells can control CMV infection in the
767 absence of T cells. *Blood* **112,** 914–915 (2008).
768 13. Orr, M., Murphy, W. & Lanier, L. 'Unlicensed' natural killer cells dominate
769 the response to cytomegalovirus infection. *Nature immunology* **11,** 321–327
770 (2010).
771 14. Smith, H. R. C. *et al.* Recognition of a virus-encoded ligand by a natural killer
772 cell activation receptor. *Proceedings of the National Academy of Sciences of*
773 *the United States of America* **99,** 8826–8831 (2002).
774 15. Li, T. *et al.* Respiratory Influenza Virus Infection Induces Memory-like Liver
775 NK Cells in Mice. *J. Immunol.* **198,** 1242–1252 (2017).
776 16. Dou, Y. *et al.* Influenza vaccine induces intracellular immune memory of
777 human NK cells. *PLoS ONE* **10,** e0121258 (2015).
778 17. Gillard, G. O. *et al.* Thy1+ NK [corrected] cells from vaccinia virus-primed
779 mice confer protection against vaccinia virus challenge in the absence of
780 adaptive lymphocytes. *PLoS Pathog.* **7,** e1002141 (2011).
781 18. Reeves, R. K. *et al.* Antigen-specific NK cell memory in rhesus macaques.
782 *Nature immunology* **16,** 927–932 (2015).

783 19. Gordon, C. L. *et al.* Tissue reservoirs of antiviral T cell immunity in persistent
784 human CMV infection. *The Journal of experimental medicine* **214,** 651–667
785 (2017).
786 20. Marquardt, N. *et al.* Human Lung NK Cells are Predominantly Comprised of
787 Highly Differentiated Hypofunctional CD69(-)CD56(dim) Cells. *J. Allergy*
788 *Clin. Immunol.* **139,** 1321–1330.e4 (2016).
789 21. Cooper, G. E., Ostridge, K., Khakoo, S. I., Wilkinson, T. M. A. & Staples, K. J.
790 Human CD49a+ Lung Natural Killer Cell Cytotoxicity in Response to
791 Influenza A Virus. *Front Immunol* **9,** 1671 (2018).
792 22. Scharenberg, M. *et al.* Influenza A Virus Infection Induces
793 Hyperresponsiveness in Human Lung Tissue-Resident and Peripheral Blood
794 NK Cells. *Front Immunol* **10,** 1116 (2019).
795 23. Chiesa, Della, M. *et al.* Phenotypic and functional heterogeneity of human NK
796 cells developing after umbilical cord blood transplantation: a role for human
797 cytomegalovirus? *Blood* **119,** 399–410 (2012).
798 24. Liu, L. L. *et al.* Critical Role of CD2 Co-stimulation in Adaptive Natural Killer
799 Cell Responses Revealed in NKG2C-Deficient Humans. *Cell Rep* **15,** 1088–
800 1099 (2016).
801 25. Marquardt, N. *et al.* Unique transcriptional and protein-expression signature in
802 human lung tissue-resident NK cells. *Nat Commun* **10,** 3841–12 (2019).
803 26. Emgård, J. *et al.* Oxysterol Sensing through the Receptor GPR183 Promotes
804 the Lymphoid-Tissue-Inducing Function of Innate Lymphoid Cells and
805 Colonic Inflammation. *Immunity* **48,** 120–132.e8 (2018).
806 27. Adams, N. M. *et al.* Transcription Factor IRF8 Orchestrates the Adaptive
807 Natural Killer Cell Response. *Immunity* **48,** 1172–1182.e6 (2018).
808 28. Lau, C. M. *et al.* Epigenetic control of innate and adaptive immune memory.
809 *Nature immunology* **19,** 963–972 (2018).
810 29. Cichocki, F. *et al.* ARID5B regulates metabolic programming in human
811 adaptive NK cells. *The Journal of experimental medicine* **215,** 2379–2395
812 (2018).
813 30. Foley, B. *et al.* Cytomegalovirus reactivation after allogeneic transplantation
814 promotes a lasting increase in educated NKG2C+ natural killer cells with
815 potent function. *Blood* **119,** 2665–2674 (2012).
816 31. Ray, S. J. *et al.* The collagen binding alpha1beta1 integrin VLA-1 regulates
817 CD8 T cell-mediated immune protection against heterologous influenza
818 infection. *Immunity* **20,** 167–179 (2004).
819 32. Cheuk, S. *et al.* CD49a Expression Defines Tissue-Resident CD8(+) T Cells
820 Poised for Cytotoxic Function in Human Skin. *Immunity* **46,** 287–300 (2017).
821 33. Vento-Tormo, R. *et al.* Single-cell reconstruction of the early maternal-fetal
822 interface in humans. *Nature* **563,** 347–353 (2018).
823 34. Masopust, D. *et al.* Dynamic T cell migration program provides resident
824 memory within intestinal epithelium. *The Journal of experimental medicine*
825 **207,** 553–564 (2010).
826 35. Melsen, J. E. *et al.* Human Bone Marrow-Resident Natural Killer Cells Have a
827 Unique Transcriptional Profile and Resemble Resident Memory CD8+ T Cells.
828 *Front Immunol* **9,** 1829 (2018).
829 36. Kumar, B. V. *et al.* Human Tissue-Resident Memory T Cells Are Defined by
830 Core Transcriptional and Functional Signatures in Lymphoid and Mucosal
831 Sites. *Cell Rep* **20,** 2921–2934 (2017).

832 37. Kaur, N. *et al.* T cells expanded in presence of IL-15 exhibit increased
833 antioxidant capacity and innate effector molecules. *Cytokine* **55,** 307–317
834 (2011).
835 38. Mimura, K. *et al.* Upregulation of thioredoxin-1 in activated human NK cells
836 confers increased tolerance to oxidative stress. *Cancer Immunol. Immunother.*
837 **66,** 605–613 (2017).
838 39. Levring, T. B. *et al.* Tumor necrosis factor induces rapid down-regulation of
839 TXNIP in human T cells. *Sci Rep* **9,** 16725–13 (2019).
840 40. O'Sullivan, T. E., Johnson, L. R., Kang, H. H. & Sun, J. C. BNIP3- and
841 BNIP3L-Mediated Mitophagy Promotes the Generation of Natural Killer Cell
842 Memory. *Immunity* **43,** 331–342 (2015).
843 41. Grayson, J. M., Laniewski, N. G., Lanier, J. G. & Ahmed, R. Mitochondrial
844 potential and reactive oxygen intermediates in antigen-specific CD8+ T cells
845 during viral infection. *J. Immunol.* **170,** 4745–4751 (2003).
846 42. Béziat, V. *et al.* CMV drives clonal expansion of NKG2C+ NK cells
847 expressing self-specific KIRs in chronic hepatitis patients. *Eur. J. Immunol.* **42,**
848 447–457 (2012).
849 43. Hammer, Q., Rückert, T. & Romagnani, C. Natural killer cell specificity for
850 viral infections. *Nature immunology* **19,** 800–808 (2018).
851 44. Szabo, P. A. *et al.* Single-cell transcriptomics of human T cells reveals tissue
852 and activation signatures in health and disease. *Nat Commun* **10,** 4706–16
853 (2019).
854 45. Smith, C. J., Caldeira-Dantas, S., Turula, H. & Snyder, C. M. Murine CMV
855 Infection Induces the Continuous Production of Mucosal Resident T Cells. *Cell*
856 *Rep* **13,** 1137–1148 (2015).
857 46. Morabito, K. M. *et al.* Memory Inflation Drives Tissue-Resident Memory
858 CD8+ T Cell Maintenance in the Lung After Intranasal Vaccination With
859 Murine Cytomegalovirus. *Front Immunol* **9,** 1861 (2018).
860 47. Wu, T. *et al.* Lung-resident memory CD8 T cells (TRM) are indispensable for
861 optimal cross-protection against pulmonary virus infection. *J. Leukoc. Biol.* **95,**
862 215–224 (2014).
863 48. Takamura, S. *et al.* Interstitial-resident memory CD8+ T cells sustain frontline
864 epithelial memory in the lung. *The Journal of experimental medicine* **159,**
865 jem.20190557 (2019).
866 49. Nizard, M. *et al.* Induction of resident memory T cells enhances the efficacy of
867 cancer vaccine. *Nat Commun* **8,** 15221 (2017).
868 50. Tang, H., Li, C., Wang, L., Zhang, H. & Fan, Z. Granzyme H of cytotoxic
869 lymphocytes is required for clearance of the hepatitis B virus through cleavage
870 of the hepatitis B virus X protein. *J. Immunol.* **188,** 824–831 (2012).
871 51. Andrade, F., Fellows, E., Jenne, D. E., Rosen, A. & Young, C. S. H. Granzyme
872 H destroys the function of critical adenoviral proteins required for viral DNA
873 replication and granzyme B inhibition. *EMBO J.* **26,** 2148–2157 (2007).
874 52. Dorner, B. G. *et al.* Coordinate expression of cytokines and chemokines by NK
875 cells during murine cytomegalovirus infection. *J. Immunol.* **172,** 3119–3131
876 (2004).
877 53. Swanson, B. J., Murakami, M., Mitchell, T. C., Kappler, J. & Marrack, P.
878 RANTES production by memory phenotype T cells is controlled by a
879 posttranscriptional, TCR-dependent process. *Immunity* **17,** 605–615 (2002).

880 54. Goodier, M. R. *et al.* Influenza Vaccination Generates Cytokine-Induced
881 Memory-like NK Cells: Impact of Human Cytomegalovirus Infection. *J.*
882 *Immunol.* (2016). doi:10.4049/jimmunol.1502049
883 55. van der Windt, G. J. W. *et al.* Mitochondrial respiratory capacity is a critical
884 regulator of CD8+ T cell memory development. *Immunity* **36,** 68–78 (2012).
885 56. Picelli, S. *et al.* Full-length RNA-seq from single cells using Smart-seq2. *Nat*
886 *Protoc* **9,** 171–181 (2014).
887 57. Picelli, S. *et al.* Tn5 transposase and tagmentation procedures for massively
888 scaled sequencing projects. *Genome Res.* **24,** 2033–2040 (2014).
889 58. Martin, M. Cutadapt removes adapter sequences from high-throughput
890 sequencing reads. *EMBnet.journal* **17,** 10 (2011).
891 59. Modolo, L. & Lerat, E. UrQt: an efficient software for the Unsupervised
892 Quality trimming of NGS data. *BMC Bioinformatics* **16,** 175 (2015).
893 60. Patro, R., Duggal, G., Love, M. I., Irizarry, R. A. & Kingsford, C. Salmon
894 provides fast and bias-aware quantification of transcript expression. *Nature*
895 *Methods* **14,** 417–419 (2017).
896 61. Love, M. I., Huber, W. & Anders, S. Moderated estimation of fold change and
897 dispersion for RNA-seq data with DESeq2. *Genome Biol.* **15,** 550 (2014).
898 62. Weigt, S. S. *et al.* Gene Expression Profiling of Bronchoalveolar Lavage Cells
899 Preceding a Clinical Diagnosis of Chronic Lung Allograft Dysfunction. *PLoS*
900 *ONE* **12,** e0169894 (2017).
901

Figure 1

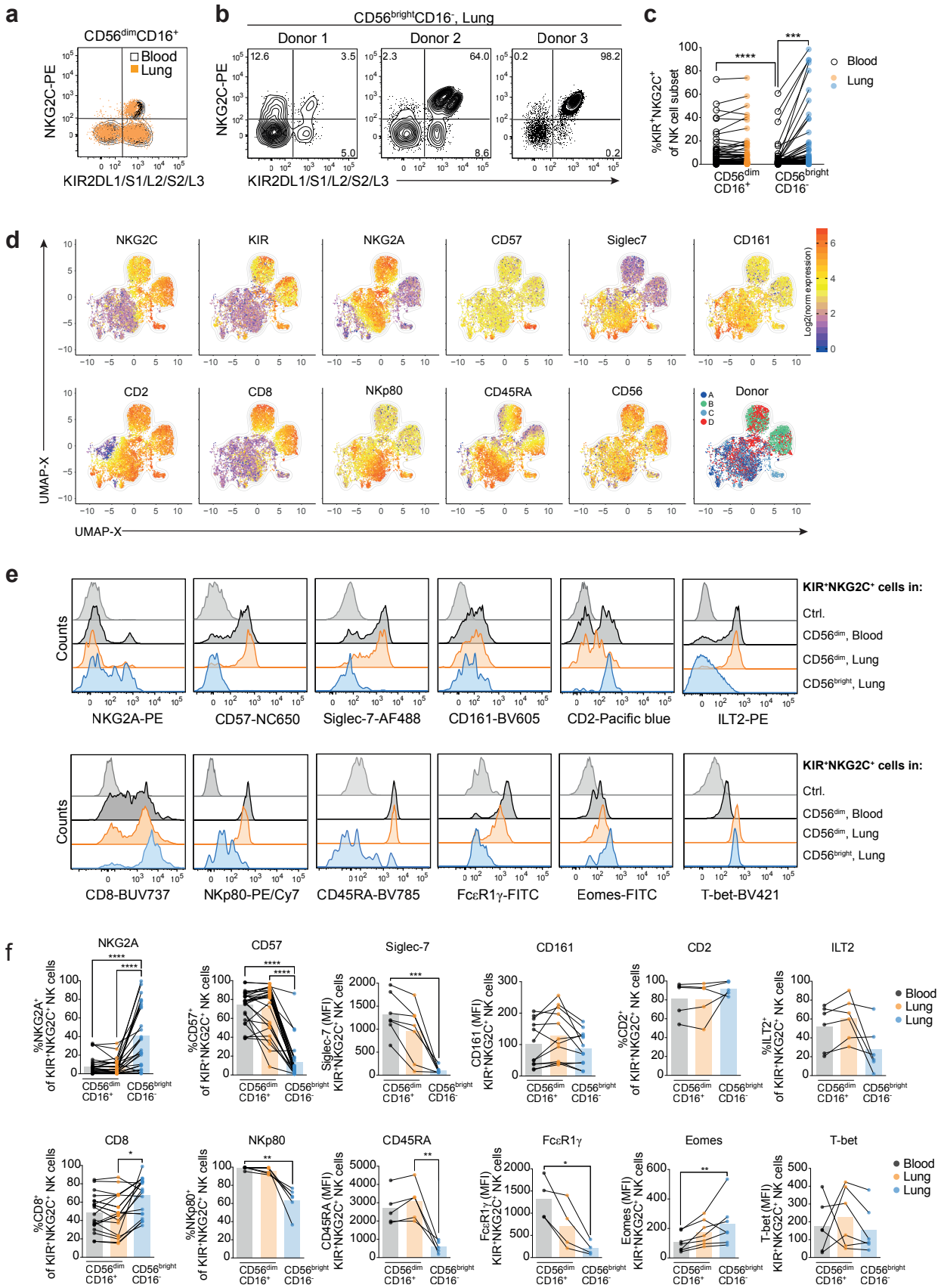
a
CD56dimCD16+
Blood
Lung
NKG2C-PE
KIR2DL1/S1/L2/S2/L3
b
CD56brightCD16-, Lung
Donor 1
Donor 2
Donor 3
12.6
3.5
5.0
2.3
64.0
8.6
0.2
98.2
0.2
c
%KIR+NKG2C+ of NK cell subset
****
***
CD56dim CD16+
CD56bright CD16-
d
NKG2C
KIR
NKG2A
CD57
Siglec7
CD161
CD2
CD8
NKp80
CD45RA
CD56
Donor
Log2(norm expression)
UMAP-X
e
KIR+NKG2C+ cells in:
Ctrl.
CD56dim, Blood
CD56dim, Lung
CD56bright, Lung
Counts
NKG2A-PE
CD57-NC650
Siglec-7-AF488
CD161-BV605
CD2-Pacific blue
ILT2-PE
CD8-BUV737
NKp80-PE/Cy7
CD45RA-BV785
FcεR1γ-FITC
Eomes-FITC
T-bet-BV421
f
%NKG2A+ of KIR+NKG2C+ NK cells
%CD57+ of KIR+NKG2C+ NK cells
Siglec-7 (MFI) KIR+NKG2C+ NK cells
CD161 (MFI) KIR+NKG2C+ NK cells
%CD2+ of KIR+NKG2C+ NK cells
%ILT2+ of KIR+NKG2C+ NK cells
%CD8+ of KIR+NKG2C+ NK cells
%NKp80+ of KIR+NKG2C+ NK cells
CD45RA (MFI) KIR+NKG2C+ NK cells
FcεR1γ (MFI) KIR+NKG2C+ NK cells
Eomes (MFI) KIR+NKG2C+ NK cells
T-bet (MFI) KIR+NKG2C+ NK cells
Blood
Lung
Lung

Figure 2

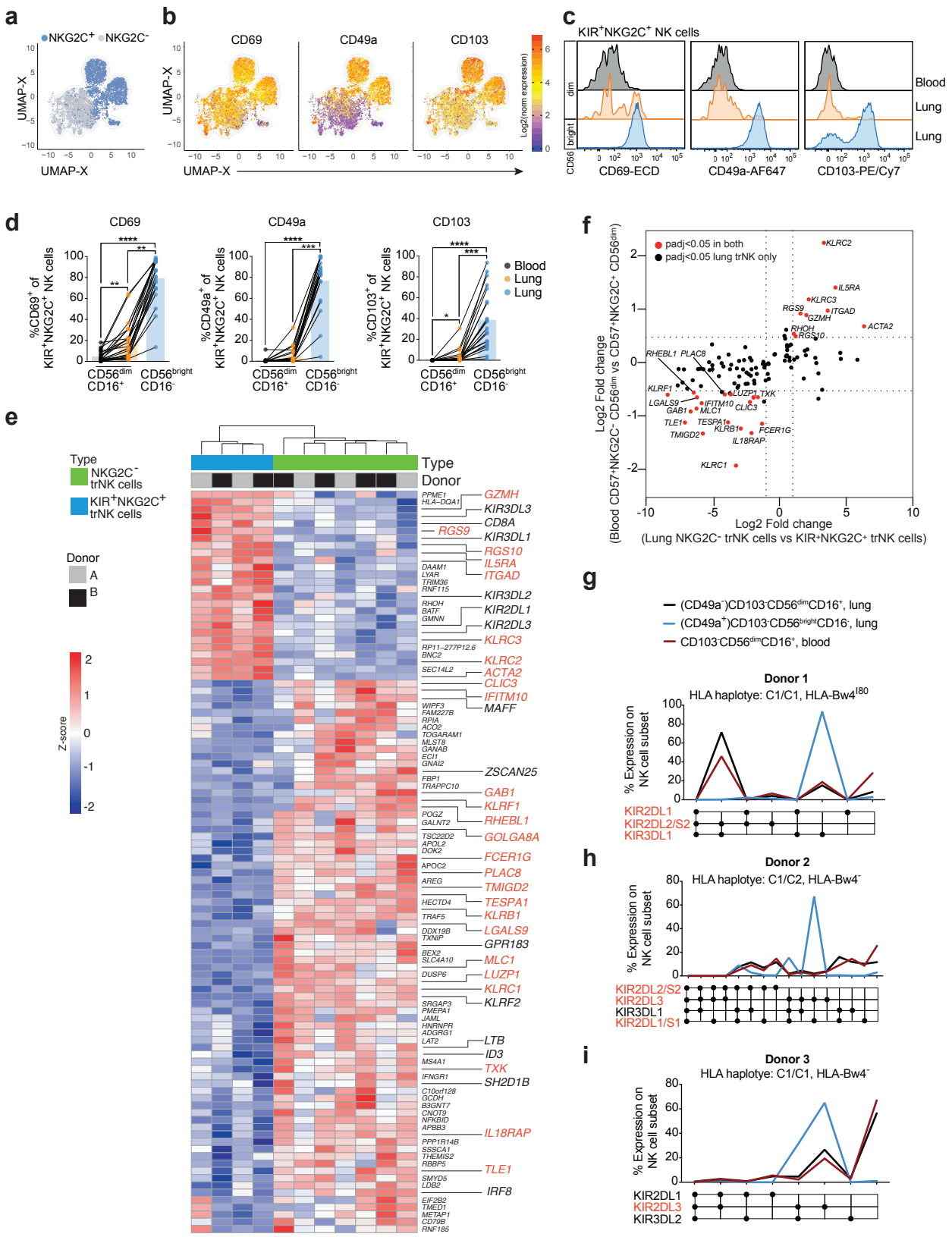
a
NKG2C+ NKG2C-
UMAP-X
UMAP-X
b
CD69
CD49a
CD103
Log2(norm expression)
UMAP-X
UMAP-X
c
KIR+NKG2C+ NK cells
dim
bright
CD56
Blood
Lung
Lung
CD69-ECD
CD49a-AF647
CD103-PE/Cy7
d
CD69
CD49a
CD103
%CD69+ of KIR+NKG2C+ NK cells
%CD49a+ of KIR+NKG2C+ NK cells
%CD103+ of KIR+NKG2C+ NK cells
Blood
Lung
Lung
CD56dim CD16+
CD56bright CD16-
e
Type
NKG2C- trNK cells
KIR+NKG2C+ trNK cells
Donor
A
B
Z-score
Type
Donor
GZMH
KIR3DL3
CD8A
RGS9
KIR3DL1
RGS10
IL5RA
ITGAD
KIR3DL2
KIR2DL1
KIR2DL3
KLRC3
KLRC2
ACTA2
CLIC3
IFITM10
MAFF
ZSCAN25
GAB1
KLRF1
RHEBL1
GOLGA8A
FCER1G
PLAC8
TMIGD2
TESPA1
KLRB1
LGALS9
GPR183
MLC1
LUZP1
KLRC1
KLRF2
LTB
ID3
TXK
SH2D1B
IL18RAP
TLE1
IRF8
f
padj<0.05 in both
padj<0.05 lung trNK only
Log2 Fold change
(Blood CD57+NKG2C- CD56dim vs CD57+NKG2C+ CD56dim)
Log2 Fold change
(Lung NKG2C- trNK cells vs KIR+NKG2C+ trNK cells)
KLRC2
IL5RA
KLRC3
RGS9
ITGAD
GZMH
RHOH
ACTA2
RGS10
RHEBL1
PLAC8
KLRF1
LUZP1
TXK
LGALS9
IFITM10
CLIC3
GAB1
MLC1
TLE1
TESPA1
KLRB1
FCER1G
TMIGD2
IL18RAP
KLRC1
g
(CD49a-)CD103-CD56dimCD16+, lung
(CD49a+)CD103-CD56brightCD16-, lung
CD103-CD56dimCD16+, blood
Donor 1
HLA haplotye: C1/C1, HLA-Bw4I80
% Expression on NK cell subset
KIR2DL1
KIR2DL2/S2
KIR3DL1
h
Donor 2
HLA haplotye: C1/C2, HLA-Bw4-
% Expression on NK cell subset
KIR2DL2/S2
KIR2DL3
KIR3DL1
KIR2DL1/S1
i
Donor 3
HLA haplotye: C1/C1, HLA-Bw4-
% Expression on NK cell subset
KIR2DL1
KIR2DL3
KIR3DL2

Figure 3

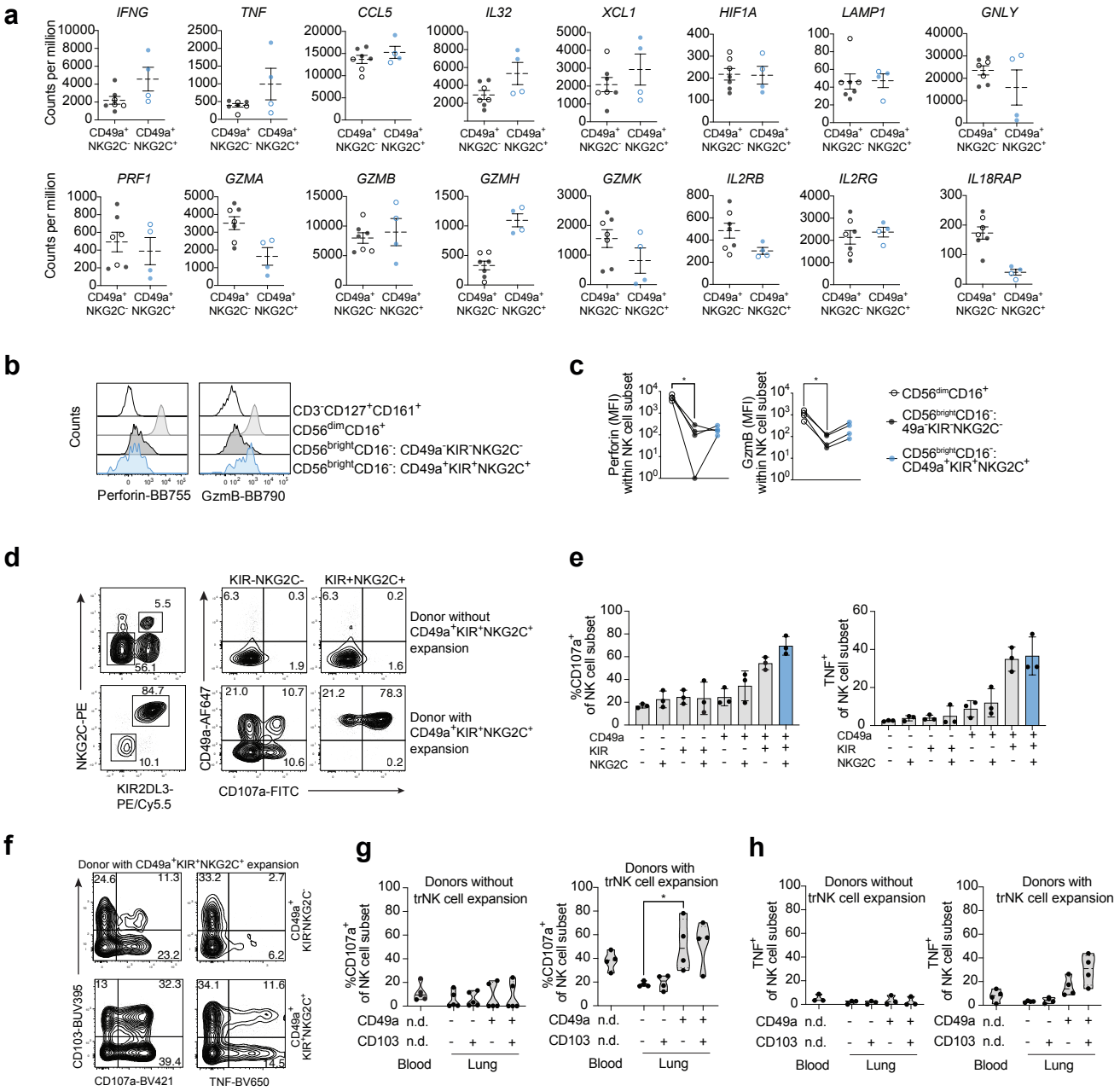
a
IFNG
TNF
CCL5
IL32
XCL1
HIF1A
LAMP1
GNLY
PRF1
GZMA
GZMB
GZMH
GZMK
IL2RB
IL2RG
IL18RAP
Counts per million
CD49a+ NKG2C-
CD49a+ NKG2C+
b
Counts
CD3-CD127+CD161+
CD56dimCD16+
CD56brightCD16-: CD49a-KIR-NKG2C-
CD56brightCD16-: CD49a+KIR+NKG2C+
Perforin-BB755
GzmB-BB790
c
Perforin (MFI) within NK cell subset
GzmB (MFI) within NK cell subset
CD56dimCD16+
CD56brightCD16-: 49a-KIR-NKG2C-
CD56brightCD16-: CD49a+KIR+NKG2C+
d
KIR-NKG2C-
KIR+NKG2C+
Donor without CD49a+KIR+NKG2C+ expansion
Donor with CD49a+KIR+NKG2C+ expansion
NKG2C-PE
KIR2DL3-PE/Cy5.5
CD49a-AF647
CD107a-FITC
e
%CD107a+ of NK cell subset
TNF+ of NK cell subset
CD49a
KIR
NKG2C
f
Donor with CD49a+KIR+NKG2C+ expansion
CD103-BUV395
CD107a-BV421
TNF-BV650
CD49a+ KIR-NKG2C-
CD49a+ KIR-NKG2C+
g
Donors without trNK cell expansion
Donors with trNK cell expansion
%CD107a+ of NK cell subset
CD49a n.d.
CD103 n.d.
Blood
Lung
h
Donors without trNK cell expansion
Donors with trNK cell expansion
TNF+ of NK cell subset

Figure 4

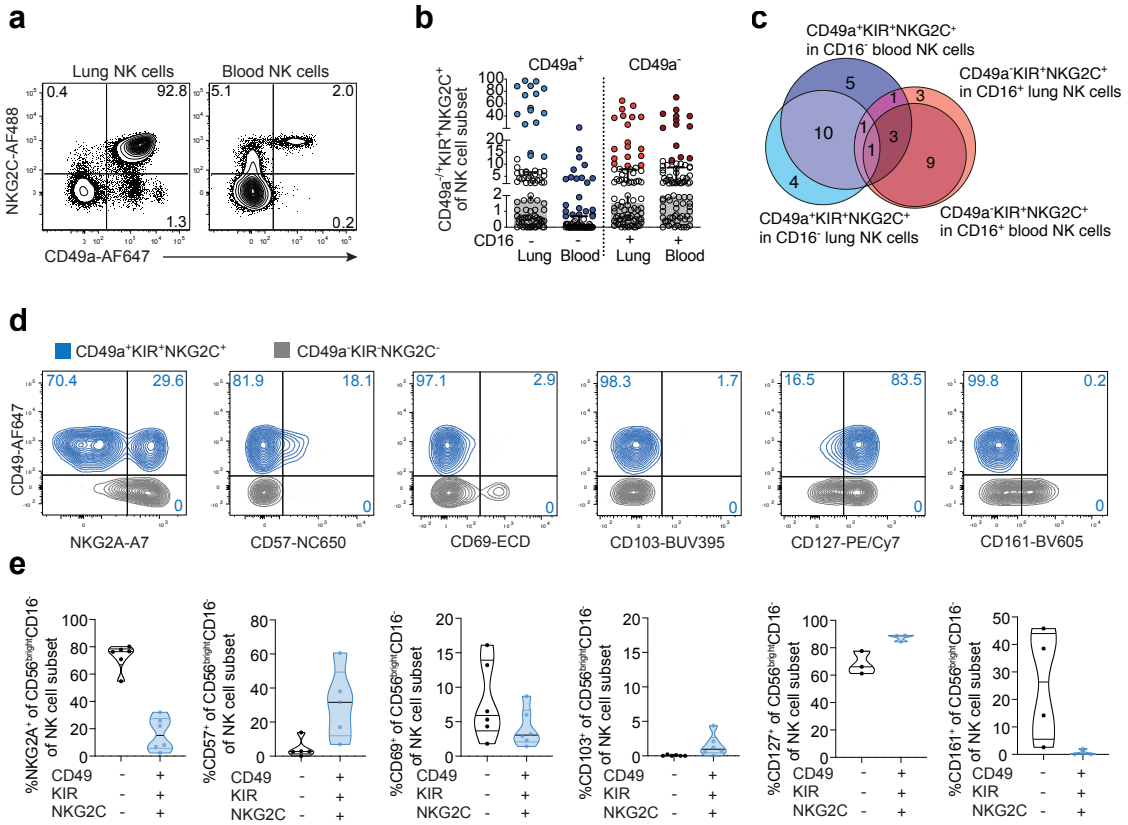
a
Lung NK cells
Blood NK cells
NKG2C-AF488
CD49a-AF647
0.4
92.8
1.3
5.1
2.0
0.2
b
CD49a+
CD49a-
CD49a-/+KIR+NKG2C+ of NK cell subset
CD16
Lung
Blood
c
CD49a+KIR+NKG2C+ in CD16- blood NK cells
CD49a-KIR+NKG2C+ in CD16+ lung NK cells
CD49a+KIR+NKG2C+ in CD16- lung NK cells
CD49a-KIR+NKG2C+ in CD16+ blood NK cells
d
CD49a+KIR+NKG2C+
CD49a-KIR-NKG2C-
CD49-AF647
NKG2A-A7
CD57-NC650
CD69-ECD
CD103-BUV395
CD127-PE/Cy7
CD161-BV605
e
%NKG2A+ of CD56brightCD16- of NK cell subset
%CD57+ of CD56brightCD16- of NK cell subset
%CD69+ of CD56brightCD16- of NK cell subset
%CD103+ of CD56brightCD16- of NK cell subset
%CD127+ of CD56brightCD16- of NK cell subset
%CD161+ of CD56brightCD16- of NK cell subset
CD49
KIR
NKG2C

Figure 5

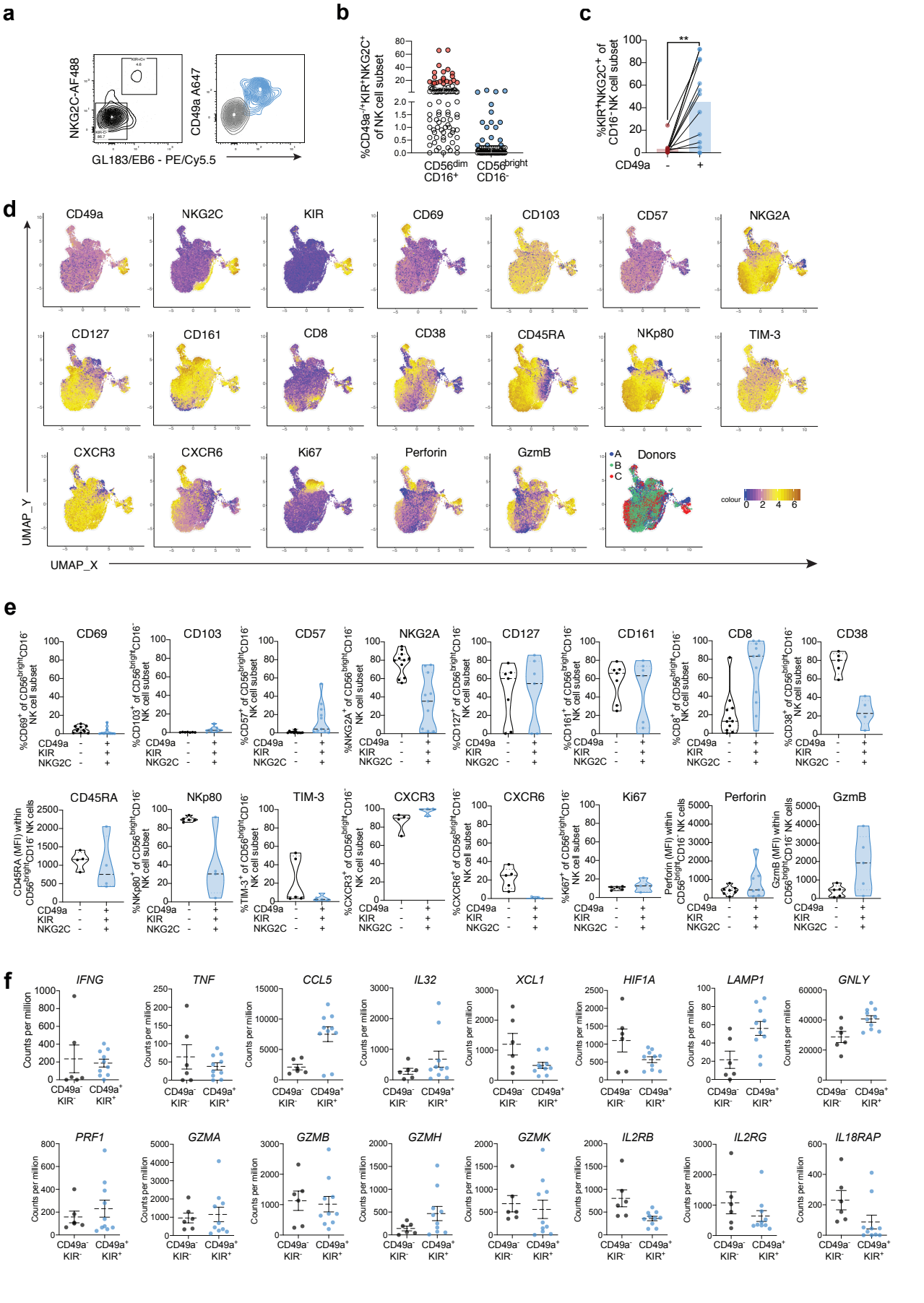
a
NKG2C-AF488
GL183/EB6 - PE/Cy5.5
CD49a A647
b
%CD49a-/+KIR+NKG2C+ of NK cell subset
CD56dim CD16+
CD56bright CD16-
c
%KIR+NKG2C+ of CD16- NK cell subset
CD49a
d
CD49a
NKG2C
KIR
CD69
CD103
CD57
NKG2A
CD127
CD161
CD8
CD38
CD45RA
NKp80
TIM-3
CXCR3
CXCR6
Ki67
Perforin
GzmB
Donors
colour
UMAP_Y
UMAP_X
e
CD69
CD103
CD57
NKG2A
CD127
CD161
CD8
CD38
CD45RA
NKp80
TIM-3
CXCR3
CXCR6
Ki67
Perforin
GzmB
CD49a
KIR
NKG2C
f
IFNG
TNF
CCL5
IL32
XCL1
HIF1A
LAMP1
GNLY
PRF1
GZMA
GZMB
GZMH
GZMK
IL2RB
IL2RG
IL18RAP
Counts per million
CD49a-
CD49a+
KIR-
KIR+

Figure 6

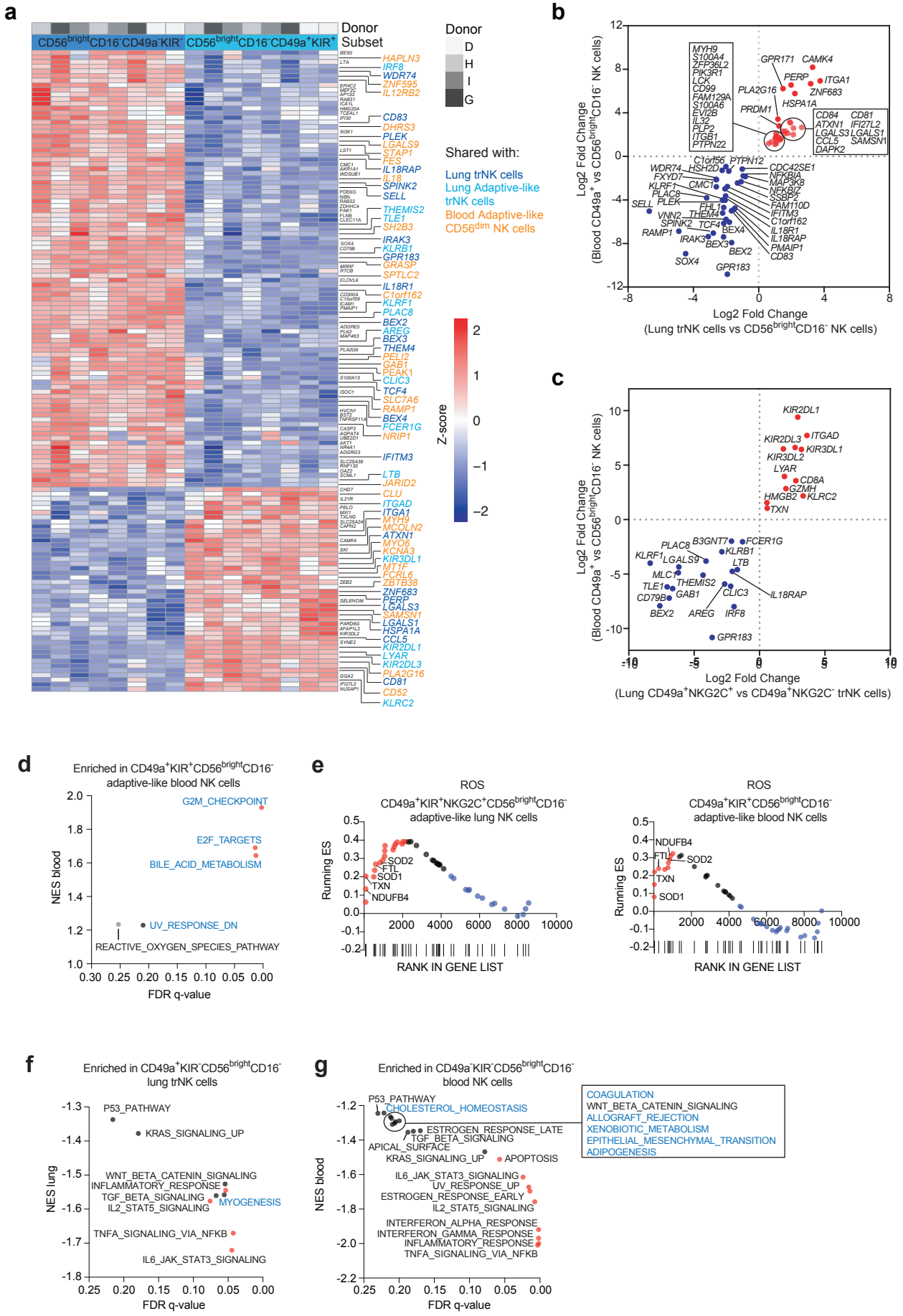
a
CD56brightCD16-CD49a-KIR-
CD56brightCD16-CD49a+KIR+
Donor Subset
Donor
D
H
I
G
Shared with:
Lung trNK cells
Lung Adaptive-like trNK cells
Blood Adaptive-like CD56dim NK cells
Z-score
b
Log2 Fold Change (Blood CD49a+ vs CD56brightCD16- NK cells)
Log2 Fold Change (Lung trNK cells vs CD56brightCD16- NK cells)
c
Log2 Fold Change (Blood CD49a+ vs CD56brightCD16- NK cells)
Log2 Fold Change (Lung CD49a+NKG2C+ vs CD49a+NKG2C- trNK cells)
d
Enriched in CD49a+KIR+CD56brightCD16- adaptive-like blood NK cells
G2M_CHECKPOINT
E2F_TARGETS
BILE_ACID_METABOLISM
UV_RESPONSE_DN
REACTIVE_OXYGEN_SPECIES_PATHWAY
NES blood
FDR q-value
e
ROS
CD49a+KIR+NKG2C+CD56brightCD16- adaptive-like lung NK cells
Running ES
RANK IN GENE LIST
ROS
CD49a+KIR+CD56brightCD16- adaptive-like blood NK cells
f
Enriched in CD49a+KIR-CD56brightCD16- lung trNK cells
P53_PATHWAY
KRAS_SIGNALING_UP
WNT_BETA_CATENIN_SIGNALING
INFLAMMATORY_RESPONSE
TGF_BETA_SIGNALING
MYOGENESIS
IL2_STAT5_SIGNALING
TNFA_SIGNALING_VIA_NFKB
IL6_JAK_STAT3_SIGNALING
NES lung
FDR q-value
g
Enriched in CD49a-KIR-CD56brightCD16- blood NK cells
P53_PATHWAY
CHOLESTEROL_HOMEOSTASIS
ESTROGEN_RESPONSE_LATE
TGF_BETA_SIGNALING
APICAL_SURFACE
KRAS_SIGNALING_UP
APOPTOSIS
IL6_JAK_STAT3_SIGNALING
UV_RESPONSE_UP
ESTROGEN_RESPONSE_EARLY
IL2_STAT5_SIGNALING
INTERFERON_ALPHA_RESPONSE
INTERFERON_GAMMA_RESPONSE
INFLAMMATORY_RESPONSE
TNFA_SIGNALING_VIA_NFKB
COAGULATION
WNT_BETA_CATENIN_SIGNALING
ALLOGRAFT_REJECTION
XENOBIOTIC_METABOLISM
EPITHELIAL_MESENCHYMAL_TRANSITION
ADIPOGENESIS
NES blood
FDR q-value

Figure 7

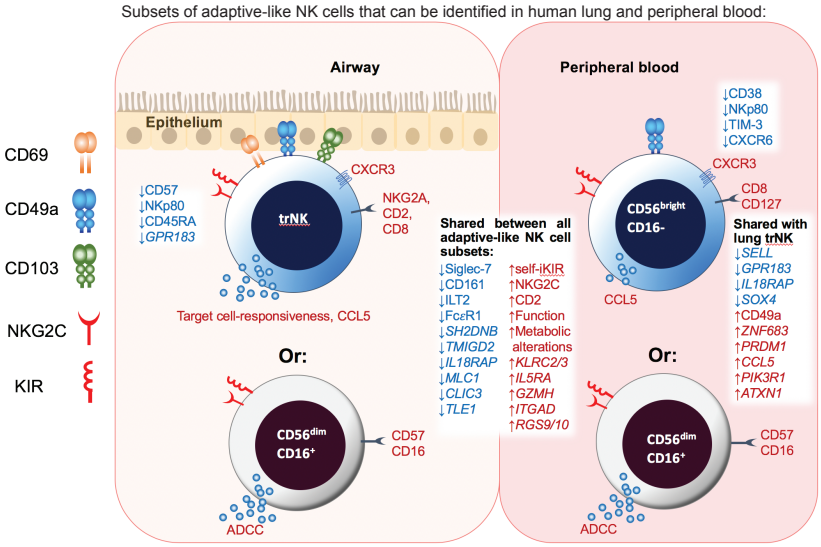
Subsets of adaptive-like NK cells that can be identified in human lung and peripheral blood:
Airway
Peripheral blood
Epithelium
CD69
CD49a
CD103
NKG2C
KIR
↓CD57
↓NKp80
↓CD45RA
↓GPR183
trNK
CXCR3
NKG2A,
CD2,
CD8
Target cell-responsiveness, CCL5
Or:
CD56dim
CD16+
CD57
CD16
ADCC
Shared between all adaptive-like NK cell subsets:
↓Siglec-7
↓CD161
↓ILT2
↓FcεR1
↓SH2DNB
↓TMIGD2
↓IL18RAP
↓MLC1
↓CLIC3
↓TLE1
↑self-iKIR
↑NKG2C
↑CD2
↑Function
↑Metabolic alterations
↑KLRC2/3
↑IL5RA
↑GZMH
↑ITGAD
↑RGS9/10
↓CD38
↓NKp80
↓TIM-3
↓CXCR6
CXCR3
CD56bright
CD16-
CD8
CD127
CCL5
Shared with lung trNK
↓SELL
↓GPR183
↓IL18RAP
↓SOX4
↑CD49a
↑ZNF683
↑PRDM1
↑CCL5
↑PIK3R1
↑ATXN1
Or:
CD56dim
CD16+
CD57
CD16
ADCC

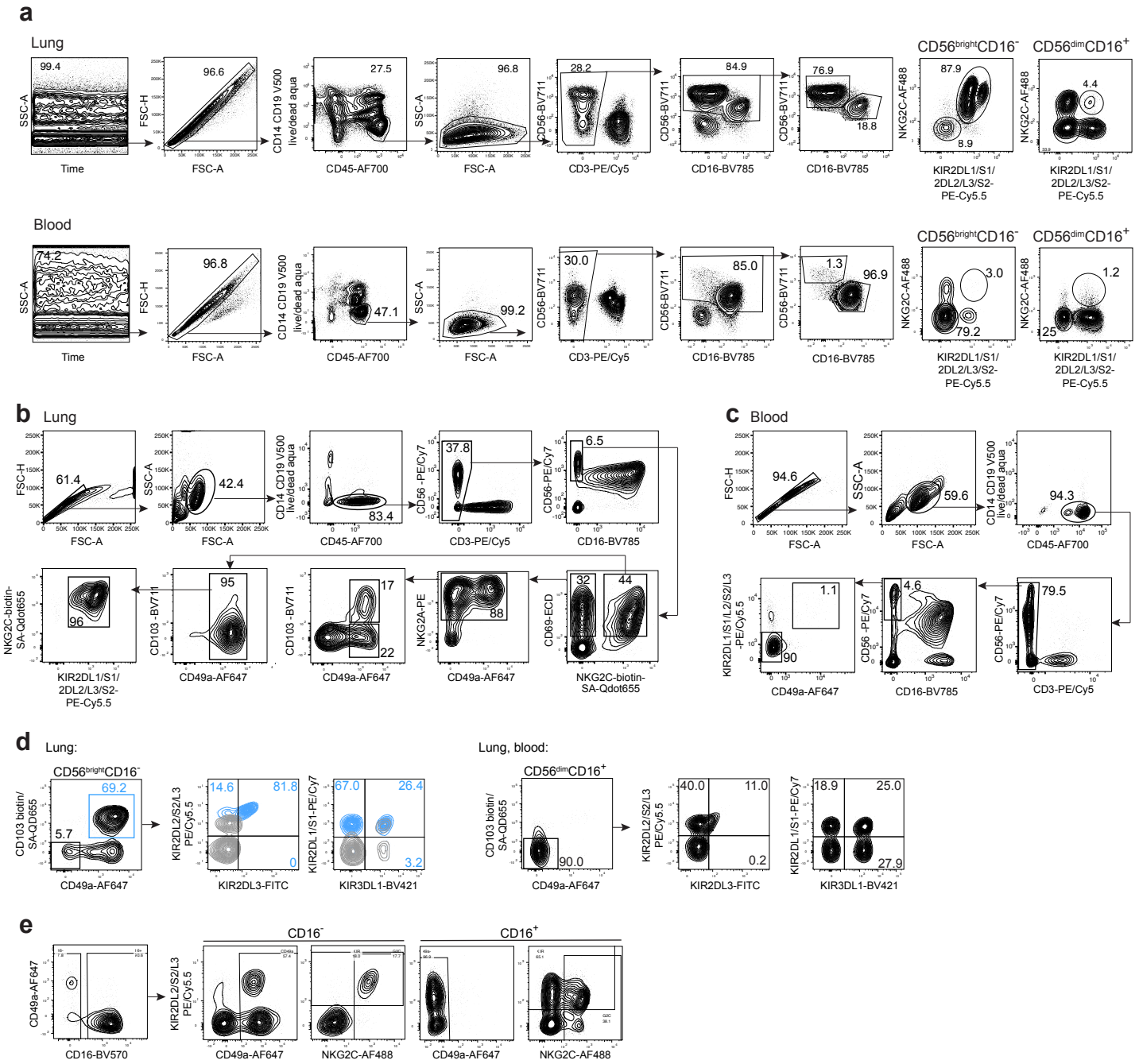

Supplementary Figure 1: Identification of adaptive-like NK cell subsets in human lung and peripheral blood. **(a)** Gating strategy to identify KIR^{+}NKG2C^{+} NK cells in human lung (upper panel) and blood (lower panel) (related to Fig. 1, 2a-d, 3b). **(b)** Gating strategy for sort for RNA sequencing analysis of lung (related to Fig. 2e,f, 3a) and **(c)** healthy blood NK cells (related to Fig. 5f, 6). **(d)** Gating strategy for single KIR analysis on CD56^{bright}CD16^{-} lung NK cells (left panel) and CD56^{dim}CD16^{+} NK cells in lung and blood (right panel) (related to Fig. 2g-i). **(e)** Gating strategy for identification of outliers within the CD16^{-} and CD16^{+} NK cell subsets (related to Fig. 4b,c).

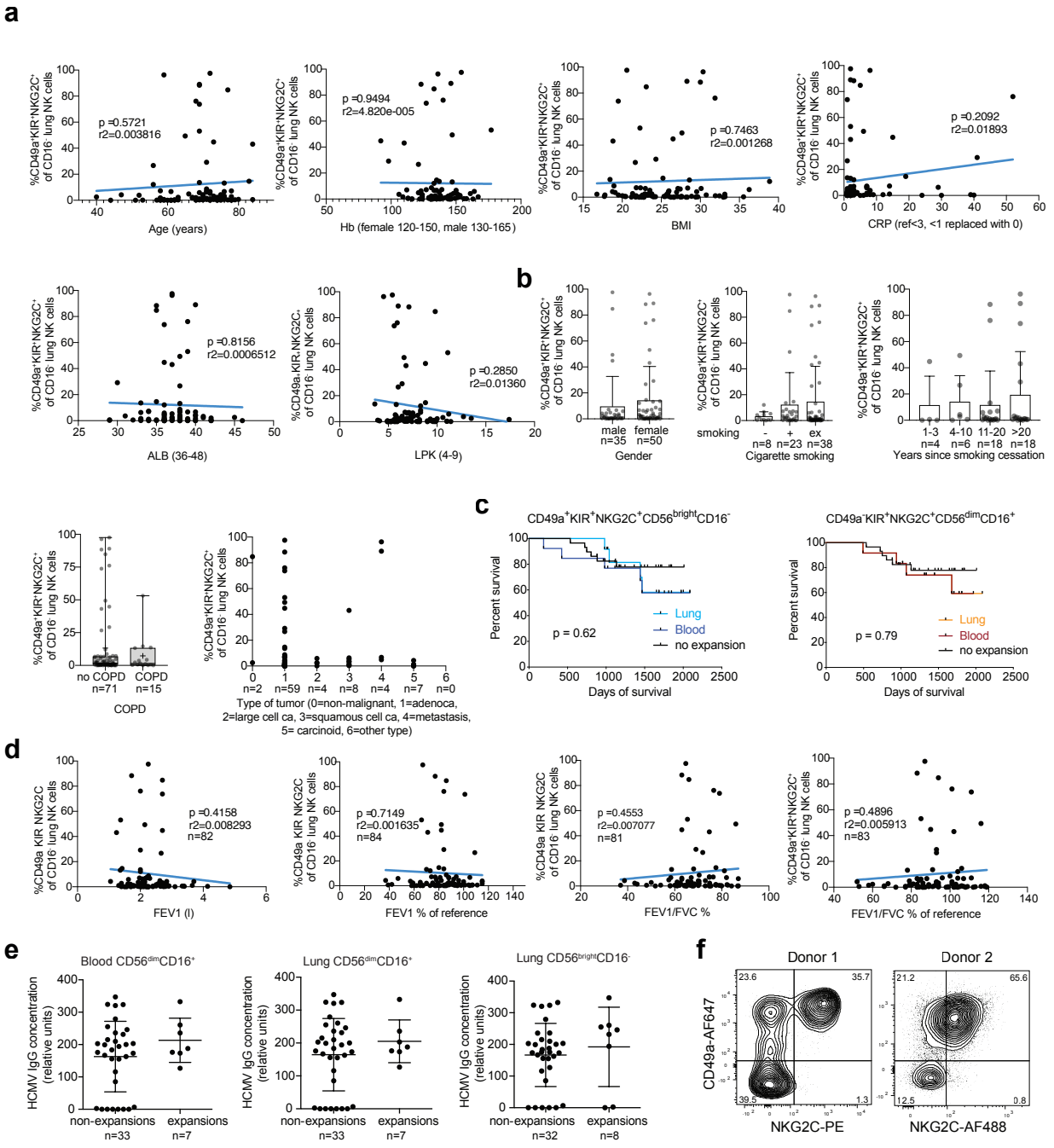

Supplementary figure 2: Association of adaptive trNK cells and patient characteristics. **(a)** Linear regression analysis of the frequency of CD49a^{+}KIR^{+}NKG2C^{+} cells among CD16^{-} lung NK cells versus age, hemoglobin (Hb) levels, body mass index (BMI), c-reactive protein (CRP) levels, albumin (ALB) levels, and leucocyte count (LPK) (n =86). **(b)** Frequencies of CD49a^{+}KIR^{+}NKG2C^{+}NK cells among CD16^{-} lung NK cells versus gender, cigarette smoking status, years since cigarette smoking cessation, chronic obstructive pulmonary disease (COPD) status, and type of tumor. Mean +/- SD is shown. **(c)** Days of survival in donors with CD49a^{+}KIR^{+}NKG2C^{+}CD56^{bright}CD16^{-} NK cell expansions in blood and/or lung (left plot) and in donors with CD49a^{+}KIR^{+}NKG2C^{+}CD56^{bright}CD16^{-} NK cell expansions in blood and/or lung (right plot) (n=57). **(d)** Linear regression analysis of FEV1 (l), FEV1 % of reference, FEV1/FV%, and FEV1/FVC % of reference is shown. **(e)** HCMV IgG concentration in plasma from donors with or without KIR^{+}NKG2C^{+}CD56^{dim}CD16^{+} expansions in blood (left) and lung (middle) and in donors with KIR^{+}NKG2C^{+}CD56^{dim}CD16^{+} expansions in in lung (right). **(f)** Expression of NKG2C and CD49a on CD56^{bright}CD16^{-} NK cells from the two HCMV-seronegative donors in (e) demonstrate adaptive-like expansions of CD56^{bright}CD16^{-} NK cells in the absence of HCMV seroconversion.

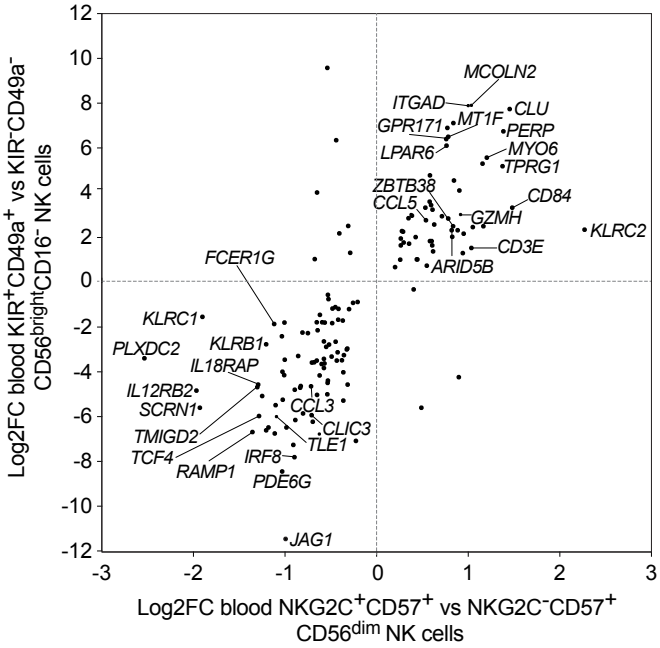

Supplementary Figure 3: Comparison of DEGs between blood CD49a$^+$KIR$^+$ CD56^{bright}CD16$^-$ NK cells and CD57$^+$NKG2C$^+$CD56^{dim} NK cells. Log2-fold changes in gene expression for shared significantly differentially expressed genes between blood CD49a$^+$KIR$^+$ and CD49a$^-$KIR$^-$ CD56^{bright}CD16$^-$ NK cells (y-axis) and CD57$^+$NKG2C$^+$ and CD57$^+$NKG2C$^-$ CD56^{dim} NK cells (x-axis). Data for CD56^{dim} NK cells are from GSE117614 (Cichocki et al).

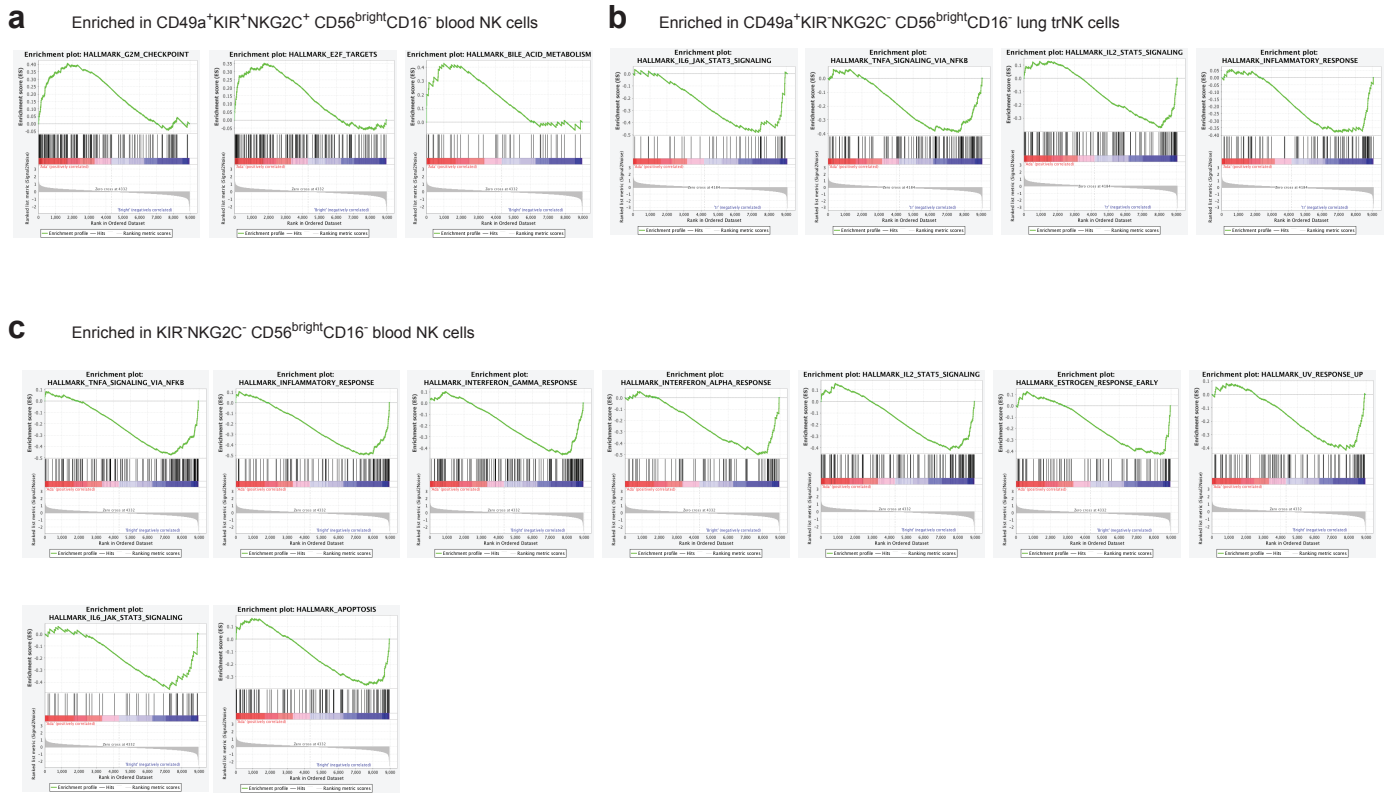

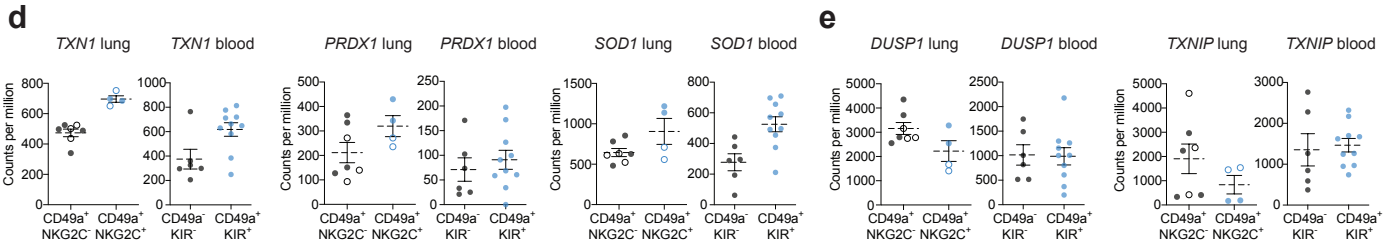

Supplementary Figure 4: Distinct pathways are enriched in adpative-like CD49a$^+$KIR$^+$NKG2C$^+$CD56^{bright}CD16$^-$ NK cells in lung and blood at transcript level. (a) Enrichment plots for pathways enriched in CD49a$^+$KIR$^+$NKG2C$^+$CD56^{bright}CD16$^-$ adaptive-like blood NK cells. **(b)** Enrichment plots for pathways enriched in CD49a$^-$KIR$^+$NKG2C$^+$CD56^{bright}CD16$^-$ (non-adaptive) lung NK cells.**(c)** Enrichment plots for pathways enriched in CD49a$^-$KIR$^-$NKG2C$^-$CD56^{bright}CD16$^-$ (non-adaptive) blood NK cells.**(d, e)** Gene expression levels in non-adaptive (CD49a$^+$KIR$^-$NKG2C$^-$CD56^{bright}CD16$^-$,CD49a$^-$KIR$^-$NKG2C$^-$CD56^{bright}CD16$^-$) and adaptive-like (CD49a$^+$KIR$^+$NKG2C$^+$CD56^{bright}CD16$^-$) NK cells in lung and blood, respectively, for genes having been reported to be upregulated **(d)** or downregulated **(e)** in cytokine-activated T cells. Mean +/- SEM is shown.